nature communications

Article

https://doi.org/10.1038/s41467-025-57581-4

A WYL domain transcription factor regulates *Lactiplantibacillus plantarum* intestinal colonization via perceiving c-di-GMP

Received: 20 June 2024

Accepted: 24 February 2025

Published online: 04 March 2025

Check for updates

Quan Guo[1,2,4], Guangqiang Wang[3,4], Leijie Zheng[1,2,4], Hui Xue[1,2], Ruimin Wang[1,2], Yajing Fang[1,2] & Jiachao Zhang[1,2]

Cyclic diguanosine monophosphate (c-di-GMP) functions as a crucial bacterial second messenger to control diverse biological functions. Although numerous studies have reported the health effects of *Lactiplantibacillus plantarum*, the regulatory role of c-di-GMP in *L. plantarum* remains elusive. Here we show that c-di-GMP functions as an important signal molecule for intestinal colonization of *L. plantarum*. The intracellular c-di-GMP pool in this probiotic is governed principally by the diguanylate cyclases DgcB, DgcC, and DgcD and the phosphodiesterases PdeA and PdeD. Moreover, we reveal that the WYL domain transcription factor MbpR is a c-di-GMP effector in *L. plantarum* WCFS1. MbpR reduces the transcription level of mucin-binding proteins (MucBPs) via binding to a special motif within the coding sequences. Perception of c-di-GMP by the WYL domain reversed the inhibitory effect of MbpR on the expression of MucBPs, resulting in increased adherence to intestinal epithelial cells by *L. plantarum*. Overall, our study provides evidence that a WYL domain transcription factor participates in probiotic colonization by sensing c-di-GMP.

Lactiplantibacillus plantarum is a lactic acid bacterium orally administrated to improve host health as numerous studies have reported the probiotic effects of *L. plantarum*[1–4]. For example, *L. plantarum* L168 was reported to ameliorate colorectal tumorigenesis by producing indole-3-lactic acid[1]. A large double-blind trial supported the use of *L. plantarum* P9 to manage chronic diarrhea in young adults[2]. Our recent study showed that the candidate probiotic *L. plantarum* HNU082 can relieve ulcerative colitis by affecting the gut microbiota and alleviate the inflammatory response induced by pathogen invasion[3,4]. The surface of the intestinal tract is covered with a thick layer of mucus, which is not only the first line of protection of the intestinal tract but also provides a desirable habitat for bacteria[5,6]. To appropriately interact with the host and impart health benefits, it is crucial for probiotics to successfully colonize in the intestinal tract[7]. However, this step is greatly challenged by harsh conditions in the gastrointestinal tract, including the presence of gastric acids in the stomach (pH 1.5–4.5), bile salts in the intestine (0.3%–0.5% w/v), and various digestive enzymes[8–10]. Additionally, survival probiotics must also compete with the indigenous bacteria inhabiting the mucosa for space and nutrition, especially in the colon, which harbors a dense bacterial population ranging from 10^{11} to 10^{12} CFU/mL[11].

The bacterial second messenger bis-(3′-5′)-cyclic guanosine monophosphate (c-di-GMP) is enzymatically synthesized by diguanylate cyclases (DGCs) harboring GGDEF domains and hydrolyzed by specific phosphodiesterases (PDEs) containing HD-GYP or EAL domains[12]. This intracellular signal modulates various bacterial biofunctions, including biofilm formation, motility, and virulence[13]. A recent study showed that elevated intracellular c-di-GMP promoted the fitness and persistence of *Pseudomonas lurida* within its host *Caenorhabditis elegans*, revealing the important role of c-di-GMP in

[1]School of Food Science and Engineering, Key Laboratory of Food Nutrition and Functional Food of Hainan Province, Hainan University, Haikou, China. [2]Collaborative Innovation Center of One Health, Hainan University, Hainan, China. [3]School of Medical Instrument and Food Engineering, University of Shanghai for Science and Technology, Shanghai, China. [4]These authors contributed equally: Quan Guo, Guangqiang Wang, Leijie Zheng.
e-mail: jiachao@hainanu.edu.cn

host-microbe symbiosis[14]. However, whether and how *L. plantarum* uses c-di-GMP to regulate colonization remains elusive.

c-di-GMP mediates bacterial biological processes via interaction with classes of specific receptors[15]. Proteins containing a PilZ domain, an inactive GGDEF domain with an inhibitory site (I site), or a degenerated EAL domain are the widely described c-di-GMP receptors[16–18]. This signal molecule can also be recognized by other types of effectors, such as proteins containing a AAA domain, MshEN domain, or REC domain[19–21]. In addition, two classes of c-di-GMP-specific riboswitches have been identified recently[22]. These results suggested that c-di-GMP receptors have substantial structural and sequence diversity. Additionally, c-di-GMP receptors usually orchestrate downstream processes via diverse regulatory mechanisms. In *Acinetobacter baumannii*, for example, c-di-GMP mediates the translation of proteins containing consecutive prolines via its interaction with elongation factor P[23]. In *Caulobacter crescentus*, c-di-GMP, when presents at elevated levels, inhibits glucose consumption by completing with (p)ppGpp to binding SmbA[24]. In *P. aeruginosa*, c-di-GMP promotes adherence and virulence by stimulating pilus assembly through the activation of FimW upon encountering surfaces[16].

Recently, a class of bacterial transcription factors carrying a conserved Trp−Tyr−Leu (WYL) sequence motif has been identified across various microbes[25–27]. Studies on the structure and function of the WYL domain transcription factors indicate that the WYL domain might serve as a module that controls the activity of transcription factors participating in bacterial immunity and DNA damage response[28–30]. Here, we report that LP_RS00300, a WYL domain transcription factor, controls the intestinal colonization behavior of *L. plantarum* WCFS1. We named this protein mucin binding protein regulator (MbpR). Interestingly, MbpR was found to bind a special motif within the coding DNA sequence (CDS), reducing the mRNA of *mbpA (LP_RS05345)* and *mbpB (LP_RS05225)*, which encode mucin binding proteins (MucBPs) and enhance the adherence of *L. plantarum* WCFS1 to the intestinal mucosa. Interaction with c-di-GMP triggered the dissociation of MbpR from the CDSs of *mbpA* and *mbpB*, consequently increasing their expression. In conclusion, our results reveal a c-di-GMP receptor that enables the intracellular c-di-GMP signal to mediate probiotic colonization.

Results

c-di-GMP Regulates the Intestinal Colonization Behavior of *L. plantarum*

As an important nucleotide second messenger, c-di-GMP plays a regulatory role in diverse bacterial biological processes[31]. To detect the c-di-GMP in *L. plantarum* WCFS1, we analyzed the intracellular extract by using liquid chromatography-mass spectrometry (LC-MS). A peak with an m/z value of 691.1023 at a retention time of 1.5 min was observed in positive-ion mode (Fig. 1a), which was consistent with the peak for the standard c-di-GMP. The peak was further verified by triple-quadrupole MS in a multiple reaction monitoring (MRM) model. The three characteristic mass transitions (m/z 691 → 540, 691 → 248, and 691 → 152) and retention time of the substance, confirmed that it was c-di-GMP (Fig. 1b). The intracellular c-di-GMP concentration of wild-type *L. plantarum* WCFS1 was detected at 32 ± 4 pmol/mg protein (three biological replicates).

To obtain insight into the regulatory role of c-di-GMP in *L. plantarum*, we overexpressed the active c-di-GMP synthetase WspR or the active c-di-GMP degradation protein RocR from *P. aeruginosa* in the wild-type strain of *L. plantarum* WCFS1. Overexpression of WspR resulted in improved cell viability of *L. plantarum* WCFS1 in pH 3.0 [degree of freedom (df) = 19, p = 7.81E-5, effect size (η^2) = 0.76, 95% Confidence Intervals (CI) = −20.64 to −7.50] or 0.2% bile salt (df = 19, p = 4.89E-7, η^2 = 0.95, 95% CI = −32.52 to −17.08) environments and increased the intracellular c-di-GMP concentration by 245% (df = 11, p = 1.36E-8, η^2 = 0.99, 95%CI = −81.55 to −65.15)(Fig. 1c–e). In contrast, overexpression of RocR led to reduced acid- (df = 19, p = 4.51E-3, η^2 = 0.62, 95% CI = 2.75 to 15.89) and bile salt- (df = 19, p = 6.80E-4, η^2 = 0.78, 95% CI = 5.78 to 21.23) resistance abilities and decreased the cellular c-di-GMP level by 87% (df = 11, p = 3.64E-5, η^2 = 0.98, 95% CI = 17.69 to 34.09)(Fig. 1c–e). The gastrointestinal tract is covered by a mucus layer that provides a desirable habitat for bacteria[5]. The mucin-secreting HT-29 cell line, a human colon cancer cell line, was used as an in vitro model to test the adhesive ability of *L. plantarum* WCFS1[32]. In trans expression of WspR facilitated the adherence of *L. plantarum* WCFS1 to HT-29 cells (df = 19, p = 7.68E-7, η^2 = 0.88, 95% CI = −5.79 to −2.97), whereas overexpression of RocR inhibited its ability to adhere to HT-29 cells (df = 19, p = 1.58E-3, η^2 = 0.65, 95% CI = 0.85 to 3.67) (Fig. 1f). Moreover, through in vivo colonization experiments, we observed that the number of *L. plantarum* cells overexpressing WspR or RocR that colonized the colon was 340% (df = 14, p = 7.93E-8, η^2 = 0.94, 95% *CI* = −1813 to −1179) and 15% (df = 14, p = 0.012, η^2 = 0.82, 95% CI = 92.89 to 727.1), respectively, of that of the wild-type strain (Fig. 1g). These results suggest that c-di-GMP promoted intestinal colonization by improving survival and adhesive ability of *L. plantarum*.

Diguanylate Cyclases and c-di-GMP-Specific Phosphodiesterases in *L. plantarum* WCFS1

By using the Basic Local Alignment Search Tool (BLAST) algorithm (https://blast.ncbi.nlm.nih.gov/Blast.cgi), we found *dgcA* (*LP_RS00050*), *dgcB* (*LP_RS12710*), *dgcC* (*LP_RS12345*), and *dgcD* (*LP_RS10755*) encodes GGDEF domains; *pdeA* (*LP_RS03290*), *pdeB* (*LP_RS03320*), *pdeC* (*LP_RS11455*), *pdeD* (*LP_RS12350*), and *pdeE* (*LP_RS03570*) encode EAL domains; but did not find any HD-GYP domain-encoding genes in the genome of *L. plantarum* WCFS1 (Fig. 2a). InterPro analysis of the protein sequences revealed the presence of multiple transmembrane domains in all GGDEF-containing proteins. In addition to a GGDEF domain, DgcA additionally possessed a PAS domain, a DDH domain, and a DHHA1 domain, which might be involved in the degradation of c-di-AMP[33]. None of the EAL domains exhibited crosslinking with other domains, thus, these proteins are predicted to be cytoplasmic.

To reveal the enzymatic activity of these c-di-GMP metabolic enzymes, the GGDEF and EAL domains were purified to investigate the in vitro DGC or PDE activity. No substrate was converted by the DgcA GGDEF domain within two hours, while approximately 38% (df = 8, p = 9.94E-6, η^2 = 0.98, 95% CI = 30.45 to 45.22), 34% (df = 8, p = 2.09E-4, η^2 = 0.93, 95% CI = 22.29 to 46.09), and 60% (df = 8, p = 2.81E-7, η^2 = 1.00, 95% CI = 54.30 to 65.97) of GTP was converted into c-di-GMP after incubation with GGDEF domains of DgcB, DgcC, and DgcD, respectively (Supplementary Fig. 1a–d). Both the PdeA (df =8, p = 4.41E-8, η^2 = 1.00, 95% CI = 92.10 to 107.1) and PdeD (df = 8, p = 1.39E-13, η^2 = 1.00, 95% CI = 96.01 to 103.60) EAL domains degraded all of the c-di-GMP to pGpG within 30 min, whereas PDE activity was not observed for the PdeB, PdeC, and PdeE EAL domains (Supplementary Fig. 1e–i).

To investigate the effect of c-di-GMP metabolic enzymes on the intracellular c-di-GMP concentration in *L. plantarum* WCFS1, we constructed single-gene deletion mutants by using clustered regularly interspaced short palindromic repeat (CRISPR)/CRISPR-associated protein 9 (Cas9)-based gene editing. Consistent with the in vitro DGC and PDE results, the intracellular c-di-GMP levels in the Δ*dgcB*, Δ*dgcC*, and Δ*dgcD* mutants decreased by 42% (df = 56, p = 5.94E-6, η^2 = 0.88, 95% CI = 18.81 to 64.86), 28% (df = 56, p = 6.97E-3, η^2 = 0.72, 95% CI = 4.52 to 50.57), and 43% (df = 56, p = 3.70E-6, η^2 = 0.91, 95% CI = 19.75 to 65.80), respectively, compared with those in the wild-type strain (Fig. 2b). In contrast, the intracellular c-di-GMP levels in the *pdeA* and *pdeD* deletion mutants increased by 74% (df = 56, p = 2.02E-12, η^2 = 0.95, 95% CI = −96.99 to −50.94) and 46% (df = 56, p = 9.02E-7, η^2 = 0.88, 95% CI = −68.62 to −22.57), respectively. In-frame deletion of *dgcA*, *pdeB*, *pdeC*, and *pdeE* did not induce a change in the intracellular c-di-GMP level in *L. plantarum* WCFS1. These results indicate that DgcB,

https://doi.org/10.1038/s41467-025-57581-4

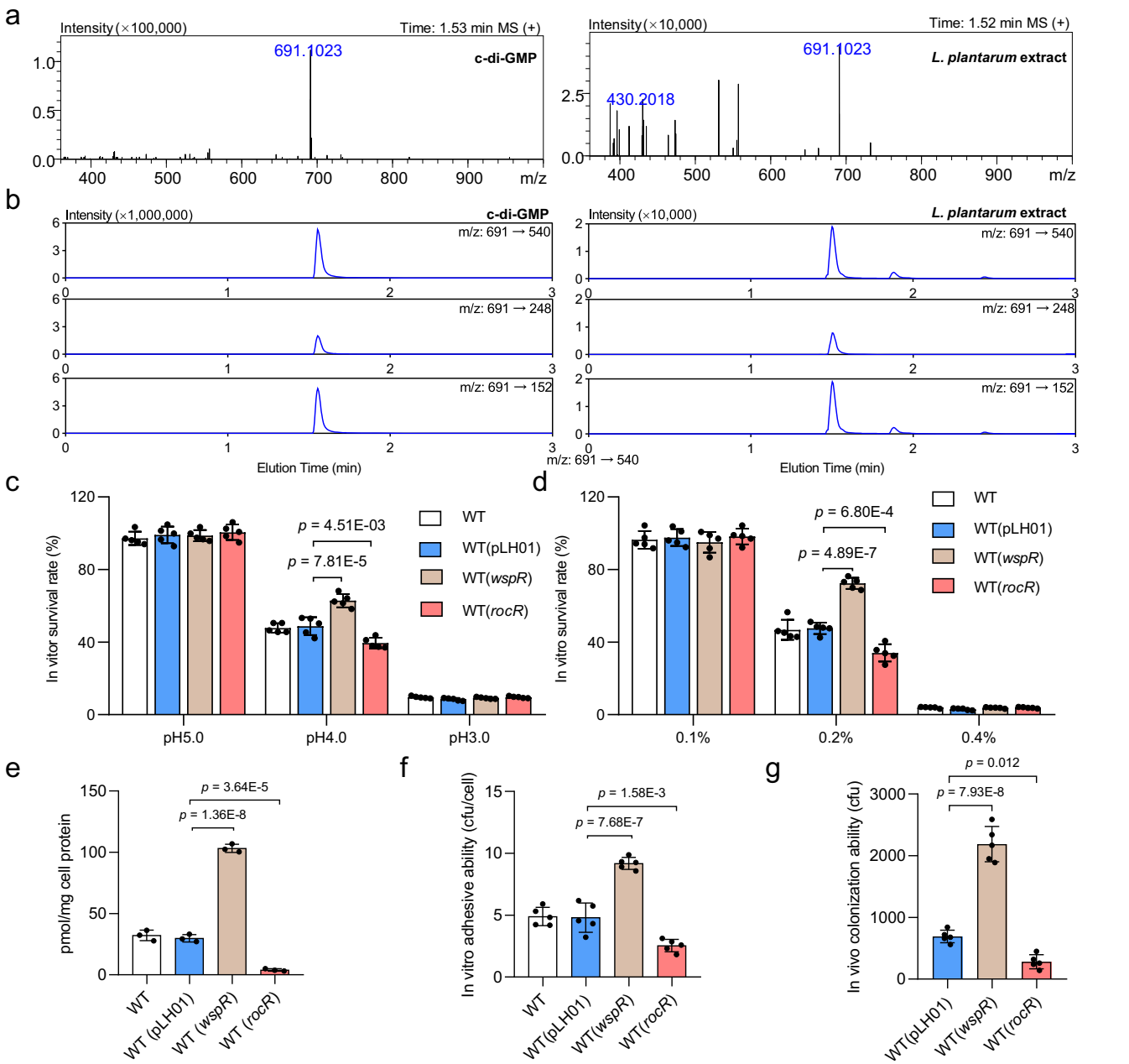

Fig. 1 | c-di-GMP promoted intestinal colonization of *L. plantarum*. **a**, **b** High-resolution mass spectra (**a**) and triple-quadrupole mass spectra in a multiple reaction monitoring model (**b**) of c-di-GMP extracted from *L. plantarum* WCFS1. Left panel: c-di-GMP standard; right panel: extracted from *L. plantarum* WCFS1. The experiments were performed three times with similar results. **c**–**g** Overexpression of active c-di-GMP synthetase WspR or the active c-di-GMP phosphodiesterase RocR influenced the acid- (**c**) and bile salt (**d**) tolerance, intracellular c-di-GMP level (**e**), adhesive ability to mucus-secreting HT-29 cells (**f**), and colonization ability within mice colon (**g**) of *L. plantarum*. The genes *rocR* and *wspR* were cloned into the pLH01 plasmid and then electroporated into the wild-type strain of *L. plantarum* WCFS1. WT(pLH01) is the wild-type strain containing pLH01 plasmid as a control vector. Data are presented as mean values ± standard deviations (SD). Error bars indicate the SD. Dots represent individual data. Statistical significance in (**c**–**g**) was determined using one-way ANOVA (**e**–**g**) with Tukey's multiple-comparison test. In (**c**, **d**, **f**, **g**): $n = 5$ biological replicates. In (**e**): $n = 3$ biological replicates. Source data are provided as a Source Data file.

DgcC, and DgcD are active DGCs, while PdeA and PdeD are active PDEs, in *L. plantarum* WCFS1.

MbpR is a c-di-GMP effector protein

To identify the underlying mechanism by which *L. plantarum* WCFS1 senses c-di-GMP to control biological functions, we conducted an affinity pull-down experiment by using biotinylated c-di-GMP to enrich potential c-di-GMP receptor from soluble protein extracts of *L. plantarum* WCFS1. Three highly enriched protein bands were identified (Fig. 3a), and these bands corresponded to PdeB, PdeC, and MbpR based on mass spectrometry analysis (Supplementary Data 1). PdeB and PdeC are EAL domain-containing proteins with conserved c-di-GMP binding sites (Fig. 2a), while MbpR harbors an HTH domain and a WYL domain (Fig. 3b). As no information on the relationship between the WYL domain and c-di-GMP has been reported, we focused on the role of MbpR in the c-di-GMP signaling system in *L. plantarum*.

The WYL domain transcription factor DriD in *Caulobacter crescentus* forms a homodimer and PafBC in *Mycobacterium smegmatis* forms a heterodimer[28,34]. We did not identify other WYL domain transcription factors in *L. plantarum* WCFS1. Thus, to investigate whether

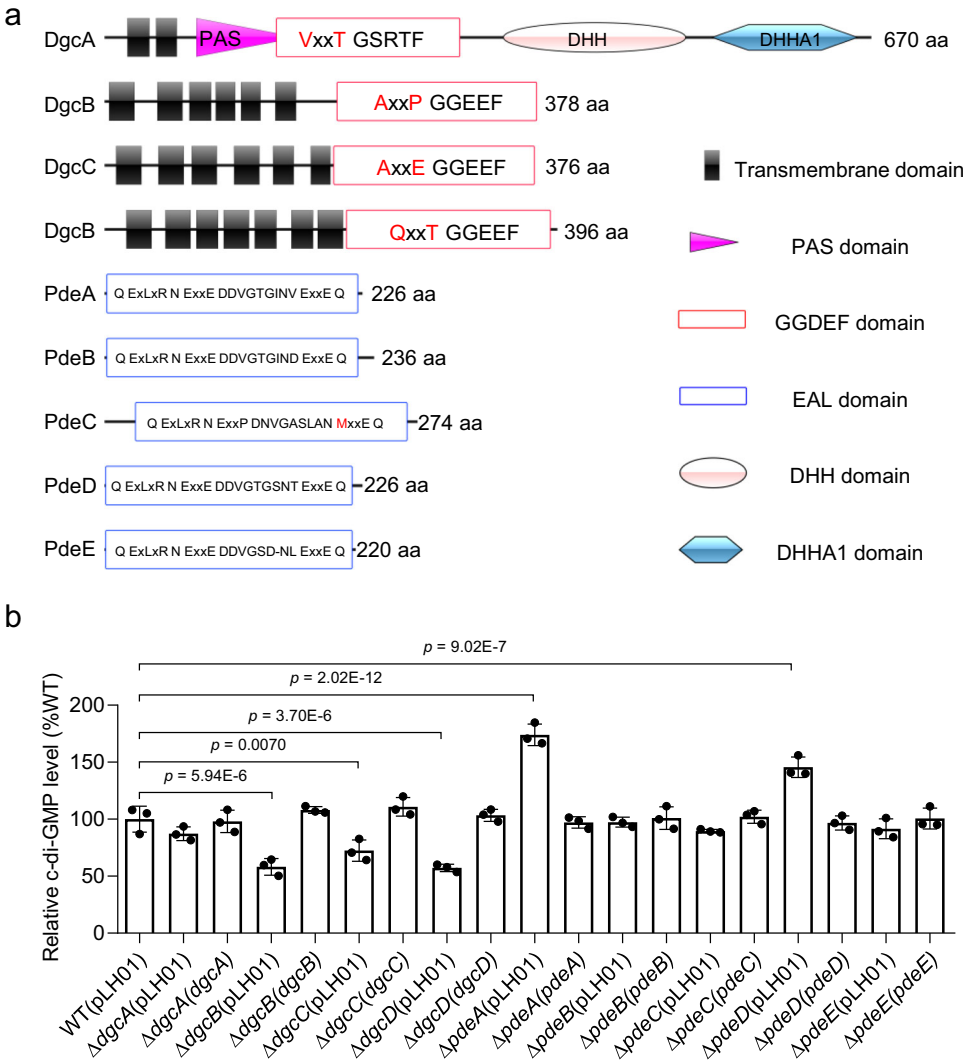

Fig. 2 | The major diguanylate cyclases and c-di-GMP phosphodiesterases in *L. plantarum* WCFS1. a Domain structure of predicted c-di-GMP-metabolizing proteins in *L. plantarum* WCFS1. aa: amino acid. **b** Intracellular c-di-GMP level in *L. plantarum* WCFS1 with single deletion of predicted c-di-GMP-metabolizing genes. Data are presented as mean values ± standard deviations (SD). Error bars indicate the SD. Dots represent individual data. The results were analyzed using one-way Analysis of Variance (ANOVA) with Tukey's multiple-comparison test ($n = 3$ biological replicates). Source data are provided as a Source Data file.

MbpR forms a homodimer, we performed a bacterial two-hybrid assay (BTHA). As shown in Fig. 3c, no interaction was observed between the MbpR and itself. Moreover, the native polyacrylamide gel electrophoresis of MbpR showed a molecular weight of 40 kDa with or without c-di-GMP (Fig. 3d), indicating that MbpR did not form a homodimer or oligomer in physiological conditions. PafC mediates protein-protein interactions with the RNA polymerase sigma factor SigA via its HTH domain[35]. However, we found that MbpR does not bind to the RpoD, the homologue of SigA in *L. plantarum* WCFS1 (Fig. 3e). Together, those results indicated that MbpR acts as a monomer.

Isothermal titration calorimetry (ITC) revealed that c-di-GMP binds MbpR at a 1:1 stoichiometry with a calculated dissociation constant (K_D) of 0.22 μM (Fig. 3f), while related nucleotides such as c-di-AMP, 3′,5′-cAMP, 3′,5′-cGMP, AMP, and GMP failed to bind, as determined by microscale thermophoresis (MST) (Supplementary Fig. 2a–f). In addition, we also purified two polypeptides containing only the WYL domain or HTH domain of MbpR and found that it is the WYL domain binds to c-di-GMP (Fig. 3g, h). To reveal how MbpR interacts with c-di-GMP, we modeled the structure of MbpR by using Alphafold2. Potential ligand-binding sites were predicted using AutoDock Vina 1.1.2 software. The lowest binding energy between the two molecules was −9.1 kcal/mol, suggesting that c-di-GMP closely contacts with MbpR. Nine amino acid residues, namely, Arg192(R192), Thr195 (T195), Tyr191 (Y191), Phe177 (F177), Tyr271 (Y271), Glu268 (E268), Tyr220 (Y220), Asp267 (D267), and Ile190 (I190), might be vital for the interaction between MbpR and c-di-GMP (Fig. 3i, j). Using protein-ligand interaction profiler (PLIP), we found that a salt bridge formed by the side chains of E268 and a guanine base (G1) of the c-di-GMP, two π-stacking interaction between the Y271 and another guanine base (G2) of the c-di-GMP, and several hydrogen bonds with the R192, Y220, and I190 residues (The model is available in Source Data). Nine single-point mutants were generated and were used to measure their ability to interact with c-di-GMP by using MST. Results showed that mutation of R192 ($df = 29$, $p = 1.03E\text{-}9$, $\eta^2 = 0.93$, 95% CI = −95.79 to −55.16) or E268 ($df = 29$, $p = 1.21E\text{-}4$, $\eta^2 = 0.89$, 95% CI = −68.49 to −4.26) resulted in a marked reduction in the c-di-GMP-binding affinity of MbpR (Fig. 3k), suggesting that these two residues directly participated in c-di-GMP binding. Sequences alignment shows that the E268 of DriD, PafB, and PafC has deviated from MbpR, however, both the R192 and E268 are conserved in the WYL domain transcription factors from *Lactiplantibacillus*, *Lactobacillus*, *Lactococcus*, *Staphylococcus*,

https://doi.org/10.1038/s41467-025-57581-4

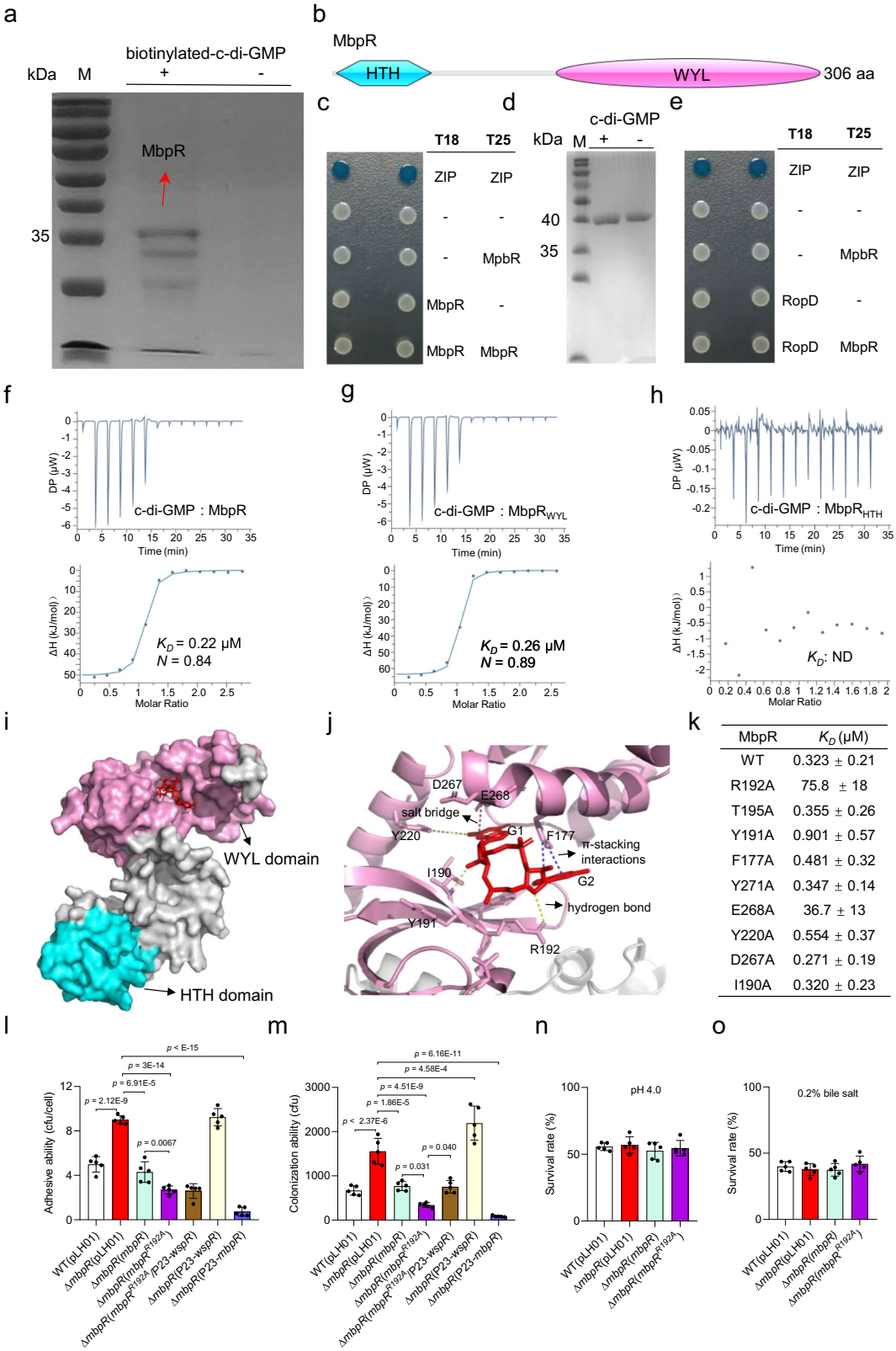

and *Enterococcus* (Supplementary Fig. 3). We thus reasonably suspected those WYL domain transcription factors might also be involved in c-di-GMP recognition.

To test the impacts of *mbpR* on the phenotypes of *L. plantarum*, we then generated an *mpbR*-null mutant by deleting the region encoding MbpR from the *L. plantarum* WCFS1 genome. In-frame deletion of *mbpR* had no impact on the intracellular c-di-GMP concentration (Supplementary Fig. 4a) but exhibited a marked increase in the ability to adhere to HT-29 cells and colonize the colon (Fig. 3l, m). Interestingly, the differences in acid- and bile salt-resistance ability between the Δ*mbpR* mutant and wild-type strains were negligible (Fig. 3n, o). In trans expression of the wild-type version of MbpR rescued the mutant phenotypes of Δ*mbpR*. At the same protein level, MbpR^{R192A} which almost lost activity to bind c-di-GMP,

Fig. 3 | MbpR is a c-di-GMP receptor in *L. plantarum*. **a** SDS-PAGE analysis of proteins enriched by biotinylated c-di-GMP (+) or control (-) from *L. plantarum* WCFS1 lysates via affinity pull-down assay. M: marker. **b** Domain structure analysis of MbpR. HTH: helix-turn-helix (HTH) domain; WYL: WYL domain. **c** Bacterial two-hybrid assay (BTHA) analysis of the interaction of MbpR and itself. **d** Native polyacrylamide gel electrophoresis of MbpR. M: Marker. **e** BTHA analysis of the interaction of MbpR and RpoD. **f**–**h** Isothermal titration calorimetry (ITC) analysis of the dissociation constants (K_D) between c-di-GMP and MbpR (**f**), or polypeptides containing only the WYL domain ($MbpR_{WYL}$) (**g**) or HTH domain ($MbpR_{HTH}$) (**h**) of MbpR. N indicates binding stoichiometry. ND: not detected. **i** Surface representation of the structural model of MbpR in complex with c-di-GMP. c-di-GMP is shown as red sticks. The figure is prepared using PyMOL. **j** The interactions between MbpR and c-di-GMP were analyzed by autodocking vina software and protein-ligand interaction profiler. The binding was visualized by Pymol. **k** Binding of c-di-GMP to MbpR mutants. The binding affinity was measured by microscale thermophoresis (MST). The K_D values are presented as mean ± standard deviations (SD) of 3 biological replicates. **l**–**o** Effects of *mbpR* on the adhesive ability to HT-29 cells (**l**), colonization ability (**m**), acid (**n**), and bile salt tolerance (**o**) of *L. plantarum* WCFS1.The data in (**a**, **c**–**h**) were performed three times with similar results. Data in (**l**–**o**) are presented as mean values ± SD. Error bars indicate the SD. Dots represent individual data. Statistical significance in **l-o** was analyzed using one-way Analysis of Variance (ANOVA) with Tukey's multiple-comparison test ($n = 5$ biological replicates). Source data are provided as a Source Data file.

even exhibited an increased effect on the complement of phenotypes (Fig.3l, m, and Supplementary Fig. 4b, c). Overexpression of *wspR* did not impact the adhesive ability of the $mbpR^{R192A}$ complemented strain to HT-29 cells, indicating that c-di-GMP promotes the adhesive ability via MbpR (Fig. 3l). However, overexpression of *wspR* enhanced the colonization ability of the $mbpR^{R192A}$ complemented strain (df = 34, $p = 0.040$, $\eta^2 = 0.82$, 95% CI = −815.0 to −13.02), suggesting that there is at least one other c-di-GMP effector contributing to the colonization phenotype different from MbpR. To gain insight into the regulatory role of *mbpR*, the transcriptomes of the wild-type, Δ*mbpR*, Δ*mbpR*(*mbpR*), and Δ*mbpR*($mbpR^{R192A}$) strain were analyzed and compared by using RNA sequencing (RNA-seq). The expressions of 94 genes were elevated while those of 3 genes were decreased (absolute value of $\log_2$ Fold Change was >1.5, $p < 0.05$) by deletion of *mbpR* (Supplementary Fig. 5a and Supplementary Data 2). Most of these differentially expressed genes were complemented by the wild-type MbpR and $MbpR^{R192A}$. Clusters of orthologous groups (COG) analysis revealed that plenty of those genes encode proteins with unknown functions or are associated with metabolism (Supplementary Fig. 5b).

MbpR binds to specific DNA sequences

Given that MbpR belongs to a member of DNA binding proteins with a HTH domain, we performed Chromatin immunoprecipitation sequencing (ChIP-Seq) to identify the binding sites for MbpR at a genome-wide scale in the *L. plantarum* WCFS1 genome using Δ*mbpR* harboring a plasmid encoding MbpR with a 3 × FLAG-tag at C-terminally. The expression of 3 × FLAG-MbpR is controlled by the P23 promoter, a strong promoter in *L. plantarum*. Western blots showed that MbpR is highly expressed under the control of P23 promoter (df = 11, $p = 5.55E\text{-}8$, $\eta^2 = 0.98$, 95% CI = −136.1 to −102.3) (Supplementary Fig. 4b, c), and overexpression of MbpR markedly inhibited the ability of *L. plantarum* to adhere HT-29 cells (df = 34, $p < E\text{-}15$, $\eta^2 = 0.99$, 95% CI = 7.00 to 9.55) and colonize gastrointestinal tract (df = 34, $p = 6.16E\text{-}11$, $\eta^2 = 0.93$, 95% CI = 1070 to 1872) (Fig. 3l, m), suggesting that 3 × FLAG-MbpR is functional. The ChIP-Seq peaks for 3 × FLAG-MbpR showed widespread occupancy across the *L. plantarum* WCFS1 chromosome (Fig. 4a). The DNA loci and enrichment fold changes for these peaks are shown in Supplementary Data 3. To experimentally verify the ChIP-Seq results, we randomly selected 3 peaks (fold enrichment >2) and a fragment with no peak as a control to perform electrophoretic mobility shift assays (EMSAs). The amount of DNA probes of peak 367, peak 336, and peaks 114 bound by MbpR increased with increasing amount of MbpR, while no DNA-protein complex was formed between the control probe and MbpR (Supplementary Fig. 6a–d), suggesting that MbpR binds the nucleoid sequence-specifically. In addition, we observed that it was the HTH domain rather than the WYL domain bound to the target DNA fragments (Supplementary Fig. 6e, f).

Multiple expectation maximization for motif elicitation (MEME) analysis of the ChIP data revealed a potential MbpR-binding motif, which was identified as 5′-YAATGGTGCCA-3′ (Fig. 4b). To test whether MbpR binds the sequence specifically, we performed EMSAs with mutated DNA fragments from peak 336 and peak 114 in which the potential MbpR-binding sites 5′-CAATGGTGACA-3′ and 5′-GAAAG GTGTCA-3′ were deleted. As expected, no DNA-protein complex was formed between MbpR and the mutated DNA probes (Supplementary Fig. 6g). Several additional peaks were also chosen for the EMSAs. The amount of DNA probe from peak 194 and peak 142 bound by MbpR increased with increasing amounts of MbpR, while deletion of the MbpR binding sequence 5′-TAATGGTGCCA-3′ or 5′- CAATGATGCCA-3′ from peak 194 and peak 142 resulted in MbpR being unable to bind the DNA probes (Supplementary Fig. 7a–d). We also added the MbpR-binding sequence of peak 144 to the DNA probe of no peak, and it was found that the addition of the MbpR-binding sequence is sufficient for binding by MbpR (Supplementary Fig. 7e). To investigate the most critical base in the MbpR-binding motif, we mutated individual nucleotide of peak 144 and found that mutation of the adenine in the second position, thymine in the seventh position, the guanosine in eighth position, or the cytosine in the tenth position led to an obvious decrease in the complex formed by MbpR and DNA probe (Fig. 4c). Using Find Individual Motif Occurrences (FIMO), a software tool for scanning DNA sequences with motifs described as position-specific scoring matrices, we identified the MbpR-binding sequences in the majority of MEME-unpredicted peaks (Supplementary Data 3). Some peaks did not harbor the MbpR-binding sequence which might be due to that MbpR binds with some sequence non-specifically at high concentrations.

Analysis of the ChIP-Seq data revealed that the FLAG-tagged MbpR signal was widely distributed at transcription start sites (TSSs) with a sharp single peak after TSSs (Fig. 4d). And 94.0% (255) and 2.2% (4) of the MbpR binding boxes were located at the CDS, or the 3′ ends of the two adjacent genes; only 3.8% (14) were enriched in the promoter region (Fig. 4e). RT-qPCR analysis was performed to determine whether MbpR represses the transcription of the bound genes. Among the ten genes tested, which all had an MbpR-binding sequence in the CDS, *LP_RS04695* (df = 8, $p = 5.66E\text{-}5$, $\eta^2 = 0.96$, 95% CI = -2.44 to -1.43), *LP_RS04100* (df = 8, $p = 1.88E\text{-}3$, $\eta^2 = 0.90$, 95% CI = −3.20 to −1.09), and *LP_RS06770* (df = 8, $p = 6.21E\text{-}3$, $\eta^2 = 0.82$, 95% CI = −2.98 to −0.70) showed a significant increase in intracellular mRNA levels upon MbpR depletion, while the other seven genes were unaffected by *mbpR* depletion (Fig. 4f). RNA-Seq analysis revealed that only 22 out of 273 genes identified by ChIP-Seq were remarkedly changed by *mbpR* deletion (Supplementary Data 3). All these differentially expressed genes were upregulated and contain an MbpR-binding sequence within their CDS region, except *LP_RS03970* which harbors an MbpR-binding sequence within its promoter. This suggests that MbpR might not function as a traditional transcriptional regulator, which is consistent with the finding that the majority of ChIP-Seq peaks are found within CDSs.

To exclude the impact of c-di-GMP and further enhance MbpR binding across the genome, we performed ChIP-Seq again with $MbpR^{R192A}$ which cannot bind c-di-GMP. 528 peaks were identified by the c-di-GMP-blind version (Supplementary Data 4). The number of

https://doi.org/10.1038/s41467-025-57581-4

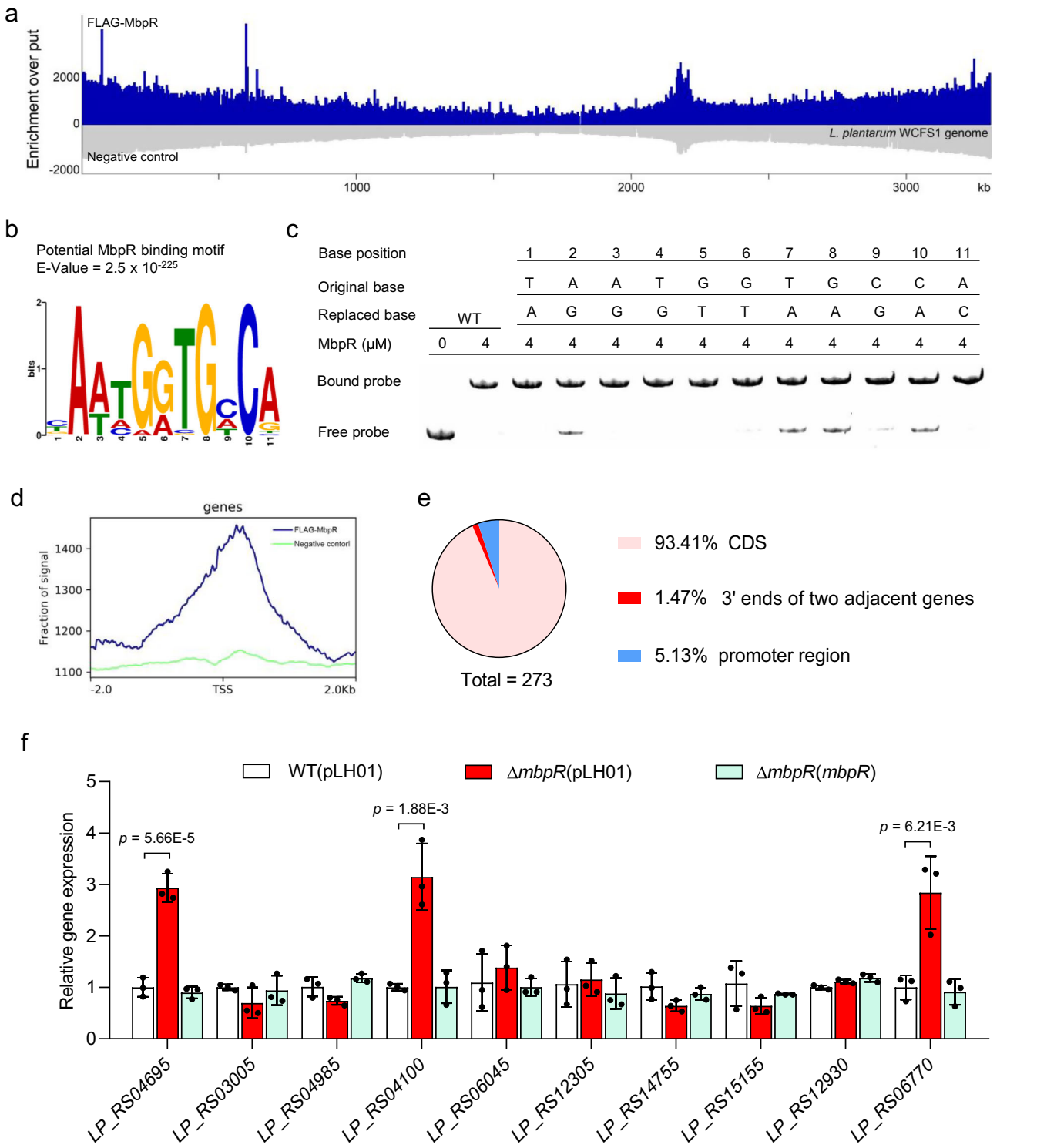

Fig. 4 | MbpR binds DNA sequence specifically. a 3 × FLAG-MbpR bound regions on the *L. plantarum* WCFS1 chromosome. **b** Potential MbpR-binding motif identified by MEME-ChIP (https://meme-suite.org/meme/doc/meme.html) based on the ChIP-Seq peaks. **c** Electrophoretic mobility shift assays (EMSA) analysis of MbpR binding to DNA probes of wild-type and mutated peak 114. **d** Chromatin immunoprecipitation sequencing (ChIP-Seq) signal density at the transcription start site. TSS: transcription start site. **e** The number of MbpR-binding sequences located at coding DNA Sequence (CDS), 3′ ends of two genes, and promoter region. The data in (**a**, **c**) was performed three times with similar results. **f** Real-time quantitative reverse transcriptase-polymerase chain reaction (RT-qPCR) analysis of MbpR bound gene expression in WT and Δ*mbpR*. Transcription levels are shown as mean ± standard deviations (SD) of 3 biological replicates. Error bars indicate the SD. Dots represent individual data. Statistical significance was analyzed using one-way Analysis of Variance (ANOVA) with Tukey's multiple-comparison test. Source data are provided as a Source Data file.

peaks identified by MbpR was substantially fewer than that of $MbpR^{R192A}$, and the majority of them coincide with the peaks found by $MpbR^{R192A}$ (Supplementary Fig. 7f), suggesting that c-di-GMP might prevent MbpR binding genome.

MbpR binding reduced the transcription level of MucBPs

Since MbpR mediated the HT-29 adherence and intestinal colonization behavior of *L. plantarum* WCFS1, we searched all the peaks for genes that might be involved in such functions and found that *LP_RS12930*

(peak 316), *mbpA* (peak 181), and *mbpB* (peak 186) encode MucBPs (Fig. 5a). LP_RS12930 is a BspA-like surface protein while its expression was not controlled by *mbpR* (Fig. 5b and Supplementary Data 2). However, the intracellular mRNA levels of *mbpA* (df = 8, $p = 3.69E\text{-}4$, $\eta^2 = 0.93$, 95% CI = −3.83 to −1.79) and *mbpB* (df = 8, $p = 1.27E\text{-}4$, $\eta^2 = 0.96$, 95% CI = −4.53 to −2.43) were significantly increased by *mbpR* depletion. Thus, we generated the Δ*mbpA*, Δ*mbpB*, and Δ*mbpAB* mutant by in-frame deletion of *mbpA*, *mbpB*, and both *mbpA* and *mbpB*, respectively. The acid- and bile salt-resistant capability was unaffected by the deletion of *mbpA* or *mbpB* (Supplementary Fig. 8a, b), while the number of Δ*mbpA*, Δ*mbpB*, and Δ*mbpAB* mutant cells that adhered to HT-29 cells were 48% (df = 19, $p = 3.16E\text{-}8$, $\eta^2 = 0.92$, 95% CI = 1.03 to 1.74), 29% (df = 19, $p = 7.19E\text{-}6$, $\eta^2 = 0.80$, 95% CI = 0.57 to 1.28), and 15% (df = 19, $p = 2.96E\text{-}9$, $\eta^2 = 0.95$, 95% CI = 1.27 to 1.98) of that of the wild-type strain, respectively (Fig. 5c). When the mucus layer on HT-29 cells was removed by pretreatment with N-acetylcysteine, the number of Δ*mbpA*, Δ*mbpB*, and Δ*mbpAB* cells that adhered to pretreated HT-29 cells was similar to that of the wild-type strain. To further confirm the mucin-binding abilities of MbpA and MbpB, we purified their mucin-binding domain and performed MST assays with mucin. Results showed that the mucin binding domain of MbpA and MbpB binds mucin with K_D values of 0.53 ± 0.17 μM and 0.69 ± 0.21 μM, respectively (Fig. 5d, e).

We then tested whether MbpR binds to the promoters of *mbpB* and *mbpA*. However, no DNA–protein complex formation was observed between MbpR and the promoters of *mbpB* and *mbpA* (Supplementary Fig. 8c, d). The MbpR binding sequences were located at the CDSs of *mbpA* and *mbpB* (Fig. 5f) and EMSAs revealed that MbpR bound the *mbpB* and *mbpA* CDS DNA probes (Fig. 5g, h). Deletion of MbpR binding sequences abolished the binding of MbpR to DNA probes (Supplementary Fig. 8e, f). Thus, we hypothesize that MbpR negatively regulates the transcription of *mbpB* and *mbpA* by binding the CDS. To confirm this, a reporter plasmid containing the *mbpB* or *mbpA* promoter and *egfp* was transformed into the wild-type strain and the Δ*mbpR* mutant. The fluorescence intensity of EGFP from the *mbpA* or *mbpB* promoter was unaffected by *mbpR* depletion (Fig. 5i, j). Insertion of MbpR-binding sequences of *mbpA* (df = 19, $p = 2.91E\text{-}10$, $\eta^2 = 0.95$, 95% CI = −4.81 to −3.30) or *mbpB* (df = 19, $p = 2.87E\text{-}8$, $\eta^2 = 0.92$, 95% CI = −2.56 to −1.52) before the *egfp* resulted in a significantly weaker EGFP fluorescence intensity in the wild-type strain compared to the Δ*mbpR* mutant (Fig. 5k, l). The EGFP level in Δ*mbpR* was complemented by the wild-type of MbpR, while $MbpR^{R192A}$ which almost lost its activity to bind c-di-GMP exhibited an enhanced effect on the complement of EGFP. We first suspected that MbpR might act on transcription elongation. Thus, we added a MbpR-binding sequence of *mbpA* between the open reading frames of EGFP and mCherry, and the fusion protein was expressed under the control of the P23 promoter. If our supposition is true, the mCherry fluorescence intensity should be enhanced by deleting *mbpR*, while the in-frame deletion of *mbpR* should have an ignorable change in the EGFP fluorescence intensity. However, we observed that *mbpR* deletion led to a similar improvement in the intensity of EGFP and mCherry (Supplementary Fig. 8g), indicating that MbpR binding reduces the transcription of the bound gene but did not cause transcription termination. As expected, the deletion of *mbpR* did not cause any changes in the intensity of EGFP and mCherry which were expressed from the *egfp-mCherry* fusion gene without MbpR-binding sequence (Supplementary Fig. 8h). To further verify that MbpR acts as a transcription inhibitor and exclude the impact of the native promoter, we performed an in vitro transcription assay using wild-type *mbpA* CDS regions or mutated *mbpA* CDS without MbpR-binding sequence as templates which are expressed under the control of the T7 promoter. MbpR reduced the mRNA synthesis of wild-type *mbpA* CDS (df = 14, $p = 1.78E\text{-}4$, $\eta^2 = 0.95$, 95% CI = 38.69 to 101.00) but did not impact that of mutated *mbpA* CDS. As expected, c-di-GMP eliminated the inhibitory effect of MbpR (df = 35.65, $p = 1.04E\text{-}3$, $\eta^2 = 0.90$, 95% CI = −87.38 to −25.11), while it did not have the same impact on $MbpR^{R192A}$ (Fig. 5m).

c-di-GMP mediated intestinal colonization of *L. plantarum* via Inhibiting MbpR Binding

As noted, elevated c-di-GMP levels promoted intestinal colonization by *L. plantarum*, and both *mbpB* and *mbpA* were involved in this effect. We then examined the impact of c-di-GMP on the MbpR binding to the *mbpA* and *mbpB* CDS DNA fragments by EMSA. The amounts of DNA probes bound by MbpR decreased with increasing amounts of c-di-GMP (Fig. 6a, b). Moreover, mutation of the c-di-GMP-binding site (R192A) eliminated the effect of c-di-GMP on the ability of MbpR to bind the *mbpA* and *mbpB* CDS (Fig. 6c, d). Similarly, c-di-GMP abolished the binding of MbpR to the other DNA fragments tested in the EMSAs (Supplementary Fig. 9a–d). To further examine the impact of c-di-GMP binding on the transcriptional levels of *mbpB* and *mbpA*, we generated a DGC-null mutant of *L. plantarum* WCFS1 by deleting the active *dgcB*, *dgcC*, and *dgcD*. The intracellular c-di-GMP concentration in the Δ3DGC mutant was below the detectable threshold (Fig. 6e). An in-frame deletion mutant strain was also constructed by deleting *pdeA* and *pdeD*, and the generated Δ2PDE mutant showed a 2.51-fold increase (df = 8, $p = 2.33E\text{-}4$, $\eta^2 = 0.93$, 95% CI = −201.8 to −100.6) in the intracellular c-di-GMP concentration. RT-qPCR analysis revealed that the transcription of *mbpA* and *mbpB* in the Δ3DGC mutant were downregulated, while that in the Δ2PDE strain were significantly elevated (Fig. 6f). EGFP fluorescence intensity from the *mbpB* and *mbpA* promoters in the wild-type, Δ2PDE, and Δ3DGC mutant strains were not significantly different (Fig. 6g, h). Thus, these results suggested that c-di-GMP promotes the expression of *mbpB* and *mbpA* by inhibiting MbpR binding.

Discussion

Based on the homology of the entire domain and the conservation of the extended signature motif, GGDEF domains can be categorized into three major classes: enzymatically functional domains (class I); enzymatically functional domains in combination with an EAL domain (class II); and enzymatically nonfunctional domains (class III)[36]. DgcB, DgcC, and DgcD could be differentiated into class I GGDEF domain, while DgcA could be differentiated into class III GGDEF domain since the GGDEF motif of DgcA is degenerated to GSRTF (Fig. 2a). As expected, the DGC activity of DgcB, DgcC, and DgcD were observed, while DgcA was not (Supplementary Fig. 1). Some degenerated GGDEF domains act as c-di-GMP receptors[13], we thus expressed the GGDEF of DgcA but did not observe its ability to bind c-di-GMP (Supplementary Fig. 10). Based on conservation of catalytic residues and loop 6, the EAL domains can be differentiated into three classes[36]. Class 1 EAL domain with conserved catalytic residues and loop6 are enzymatically active; class 2 EAL domain with conserved catalytic residues and degenerated loop6 are potentially active, whereas class 3 EAL domain with degenerated catalytic residues and loop6 are catalytically inactive. Due to the degenerated loop 6, PdeA, PdeB, PdeD, and PdeE belong to the class 2 EAL domain. PdeA and PdeD exhibited catalytic ability, while PdeB and PdeE did not (Supplementary Fig. S1). We speculate that PdeB and PdeE were enzymatically inactive or their capabilities are too weak to detect. The catalytic base of the PdeC EAL domain (the first glutamate residue in the EGVE motif) is mutated to methionine. Therefore, PdeC belongs to the class 3 EAL domain and is catalytically inactive.

Conserved features facilitate the identification of c-di-GMP synthetase or hydrolase. However, since diverse classes of c-di-GMP effectors do not share sequence or structural similarity, only a few types of c-di-GMP receptors could be discerned solely through conserved motifs, such as the ExLxR motif in the EAL domain, the RxxD motif in the GGDEF domain, and the RxxxR and (D/N)x(S/A)xxG motifs in the PilZ domain. This is particularly true for *L. plantarum*, in which no c-di-GMP effectors have been reported yet. In this study, we

https://doi.org/10.1038/s41467-025-57581-4

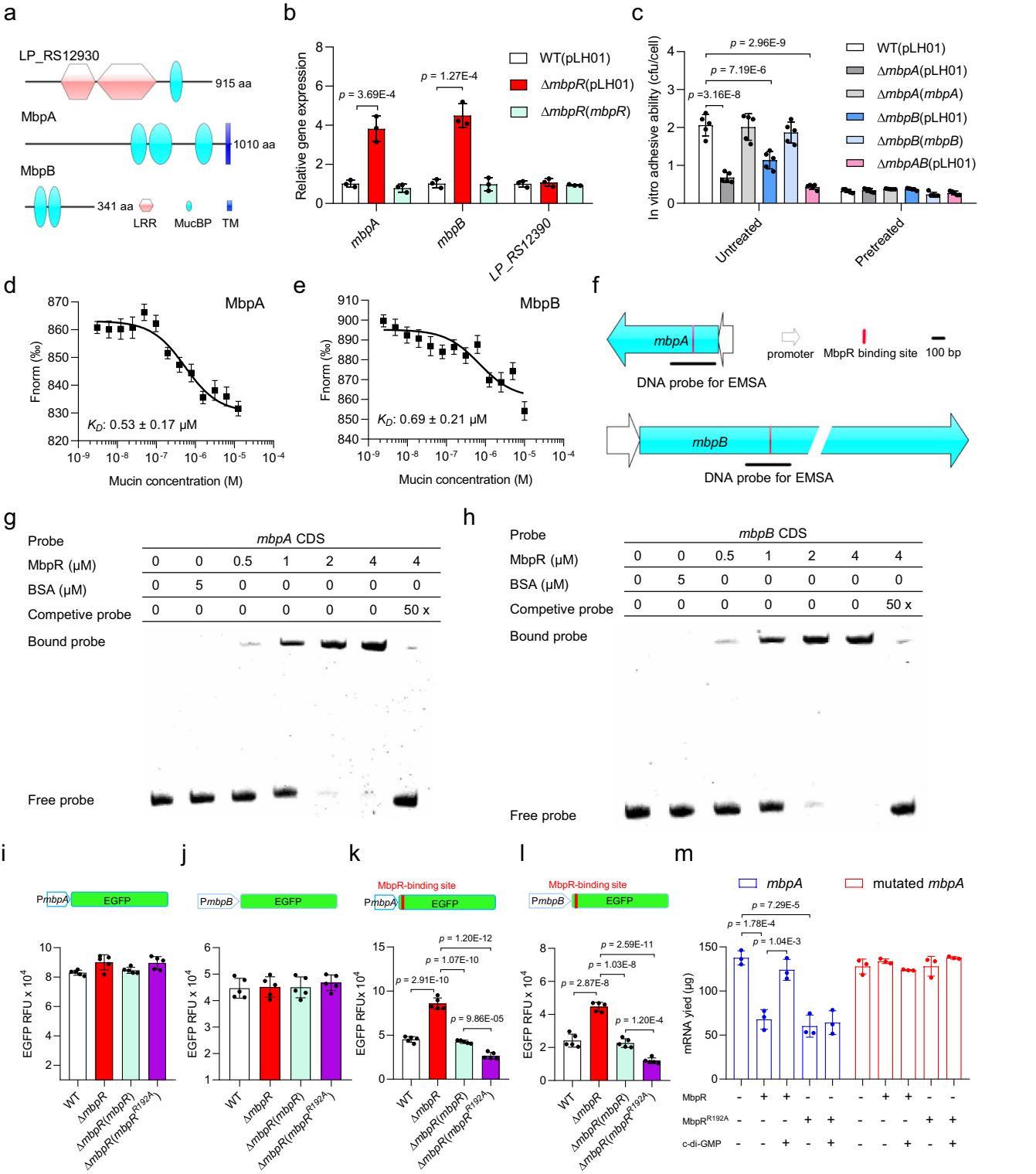

identified MbpR, a WYL domain transcription factor, as a c-di-GMP receptor protein via multiple approaches (Fig. 3). WYL domains have an Sm-like SH3 β-barrel fold, which is commonly encountered in RNA-binding proteins and is predicted to bind ligands[26]. Previous research showed the ability of the WYL domain to interact with ssDNA[27,34], and our results revealed that the WYL domain of MbpR binds to c-di-GMP with high affinity (Fig. 3f, g). These results indicated that the WYL domain might respond to different nucleic acids.

WYL domain transcription factors are frequently mentioned in connection with bacterial immunity due to their colocalization with antiphage systems, including CRISPR–Cas adaptive immunity systems or the BREX system[29,37,38]. For example, DriD in *Caulobacter crescentus* was reported to regulate DNA damage responses independent of the canonical SOS pathway[25]. CapW in *E. coli* strongly represses cyclic oligonucleotide-based anti-phage signaling system gene expression in uninfected cells[29]. BrxR in *E. fergusonii* was reported as a regulator of pEFER phage defence island[30]. These WYL regulators form a homodimer and mediate gene transcription by binding to specific sequences in promoter regions. Our results revealed that MbpR acts as a monomer and binds to the CDS rather than the promoter regions of *mbpB*

Fig. 5 | MbpR mediates expression of mucus-binding protein via impeding transcription. a Domain structure analysis of LP_RS12930, MbpA, and MbpB. MucBP: mucin-binding-protein domain; LRR: Leucine-rich repeat; TM: Transmembrane domain. **b** Relative transcription of *mbpA* and *mbpB* in *L. plantarum* wild-type and Δ*mbpR* mutant measured by real-time quantitative reverse transcriptase-polymerase chain reaction (RT-qPCR). **c** Effects of *mbpA* and *mbpB* on the ability of *L. plantarum* WCFS1 to adhere HT-29 cells. **d**, **e** MST was used to analyze the binding affinity between mucin and the mucin-binding domains of MbpA (**d**) and MbpB (**e**). Data are presented as mean values ± standard deviations (SD) of three replicates. Error bars indicate the SD. **f** Location of MbpR binding motif on the *mbpA* and *mbpB* coding DNA sequence (CDS) regions**. g, h** EMSA analysis of MbpR binding to *mbpA* (**g**) and *mbpB* (**h**) CDS regions. **i, j** EGFP expression from the *mbpA* (**i**) and *mbpB* (**j**) promoter. **k**, **l** Effect of MbpR-binding motif in the CDS region on the expression EGFP under the control of *mbpA* (**k**) and *mbpB* (**l**) promoter. The strains used in (**i**–**l**) contain reporting plasmid. **m** In vitro transcription of wild-type *mbpA* CDS and mutated *mbpA* CDS in which the MbpR-binding sequence is deleted. The mRNA yield was measured after 2 h of reaction. Data in (**b**, **c**, **i**–**m**) are presented as mean values ± SD. Error bars indicate the SD. Dots represent individual data. Statistical significance in (**b**, **c**, **m**, **i**–**l**) was analyzed using one-way ANOVA Tukey's multiple-comparison test. In (**b**, **m**): $n = 3$ biological replicates. In (**c**, **i**–**l**): $n = 5$ biological replicates. The data in (**g**, **h**) were performed three times with similar results. Source data are provided as a Source Data file.

and *mbpA* (Figs. 3, 5), thus inhibiting transcription of bound genes (Fig. 5i–l). An increasing number of transcription factors have been found to bind the CDS region in prokaryotes. For example, ChIP-Seq data revealed that the transcription factors from bacteria, including *P. aeruginosa*, *P. syringae*, and *E. coli* K-12, have 92.6% (19,707) of their binding peaks located in CDS[39]. However, the functions of CDS binding by transcription factors are little illustrated. A recent study revealed that transcription factor AlgR and VqsM interact with the CDS region and are involved in producing antisense transcripts and regulating the expression of bound genes[39]. Our research indicated that MbpR reduced the mRNA production but did not cause transcription termination of bound genes (Supplementary Fig. 8g, h). Moreover, the inhibitory effect of MbpR binding on mRNA production was observed not only in *L. plantarum* in vivo but also in the in vitro transcription assay (Fig. 5i–m). We thus speculated that MbpR might lower the transcription rate of bound genes given that the transcription elongation rate varies between regions within a gene[40,41]. To verify our hypothesis, we detected the mRNA synthesis rate of the wild-type *mbpA* CDS and mutated *mbpA* CDS without the MbpR-binding sequence under the control of the T7 promoter. It was observed that MbpR indeed weakened the transcription rate of wild-type *mbpA* CDS (Supplementary Fig. 11). Moreover, c-di-GMP eliminated the inhibitory effect of MbpR on the transcription rate of the wild-type *mbpA* CDS. Those results revealed that MbpR binding inhibited the transcription rate of the bound gene and c-di-GMP reversed the inhibitory effect of MbpR. Though our study is limited by the unresolved mechanism by which MbpR inhibits transcription rate, our study provided a glance into the function of CDS binding by transcription factors.

To establish attachment on the biotic or abiotic surfaces, many bacteria produce adhesins to allow themselves glue to the solid substrate. A critical signal controlling the processes is the second messenger c-di-GMP, which mediates the production of various adhesins in different bacteria. The most reported adhesin includes exopolysaccharides and fimbria[42,43]. In addition, some extracellular proteins such as LapA and CdrA were also secreted to form biofilm. LapA is required for the initial adhesion of *P. putida* to a surface and expression of *lapA* is under the control of intracellular c-di-GMP via the GacS/GacA two-component regulatory system[44]. The transcription of CdrA, another extracellular protein known to mediate cell-cell aggregation and biofilm maturation, is also in a c-di-GMP-dependent manner[45]. Our results revealed that c-di-GMP also mediated the expression of MucBP to adhere the mucin on intestinal epithelial cells. Those data suggested that c-di-GMP controls bacterial attachment via diverse pathways. It's worth noting that high c-di-GMP levels on the adhesive phenotype fully go through MbpR as $mbpR^{R192A}$ is fully epistatic to *wspR* overexpression (Fig. 3l). In contrast, the high c-di-GMP affects the colonization phenotype only partially through MbpR, as *wspR* overexpression increases colonization in a $mbpR^{R192A}$ background (Fig. 3m). This means that most likely there is at least one other c-di-GMP effector contributing to the colonization phenotype different from MbpR. Together, this also implies that increased adherence to mucus is not the only factor contributing to better colonization in the high c-di-GMP regime.

We analyzed the genomes of 277 *L. plantarum* strains and found though 36% of strains lack the homologous gene of *mbpA*, 99% of the strains concurrently harbor the homologous genes of *mbpR*, *dgcC*, *dgcD*, *dgcB*, and *mbpB* (Supplementary Data 5). Based on these findings, we propose a regulatory pathway in which c-di-GMP controls intestinal colonization of *L. plantarum* (Fig. 6i). MbpR binds to the MucBPs CDS and reduces their transcriptional at low level of c-di-GMP. After sensing unknown signals, the intracellular c-di-GMP level elevated and that was perceived by the WYL domain of MbpR. This interaction causes MbpR to detach from the CDSs of MucBPs, thereby promoting the expression of MucBPs and facilitating the colonization of *L. plantarum*. While sugar, bile salts, and bicarbonate were shown to affect intracellular c-di-GMP level[46–48], certain details in this model remain to be elucidated, particularly the exact signals detected by GGDEF/EAL domain-containing proteins in *L. plantarum*. However, the model offers a foundation for understanding the intestinal colonization of *L. plantarum*. In conclusion, our results may inspire further studies to reveal the regulatory roles of c-di-GMP in the probiotic-microbe interaction.

Methods

Bacterial growth conditions

The bacterial strains and plasmids used in this work are listed in Supplementary Data 6. All primers were synthesized by GENEWIZ Inc. and listed in Supplementary Data 7. *L. plantarum* WCFS and its derivatives were cultured at 37 °C in de Man, Rogosa, Sharpe (MRS) medium. When required, the following antibiotics were added: chloramphenicol, 10 μg/mL; erythromycin, 10 μg/mL. *E. coli* strains were grown in lysogeny broth (LB) culture medium. For selection, 50 μg/mL of kanamycin or 20 μg/mL of chloramphenicol were supplemented when necessary.

Preparation of electrocompetent cells and transformation

Briefly, 2 mL of the overnight culture of *L. plantarum* was inoculated into 100 mL MRS supplemented with 0.2 M sucrose and 3 % glycine at 37 °C. The cells were grown to an optical density of 600 nm (OD_{600}) = 0.4–0.6. Cells were sequentially washed twice with 1 mM $MgCl_2$ and once with electroporation buffer (952 mM sucrose, 3.5 mM $MgCl_2$)[49], and resuspended in 1 mL of electroporation buffer. 200 ng of pLH01 plasmid and 60 μL of electrocompetent cells were mixed and transferred into a 2 mm cuvette (Bio-Rad, USA). The electroporation was performed with GenePulser Xcell (Bio-Rad, USA) with the following parameters: 2.1 kV, 200 Ω, 25 μF. One milliliter of recovery buffer (MRS with 0.5 M sucrose and 0.1 M $MgCl_2$) was added into the cuvette and transferred into 2 mL of centrifuge tube. After incubating at 37 °C for 3 h, the cells were spread on MRS agar plates containing 10 μg/mL chloramphenicol. The clone containing pLH01 plasmid was confirmed by PCR using the primer listed in Supplementary Data 7.

Genome editing and complementation

To generate genome-editing plasmids, the guide RNA framework and two 1000 bp fragments flanking target gene were amplified from pHSP02 plasmid[49] and *L. plantarum* WCFS1, respectively, by PCR using

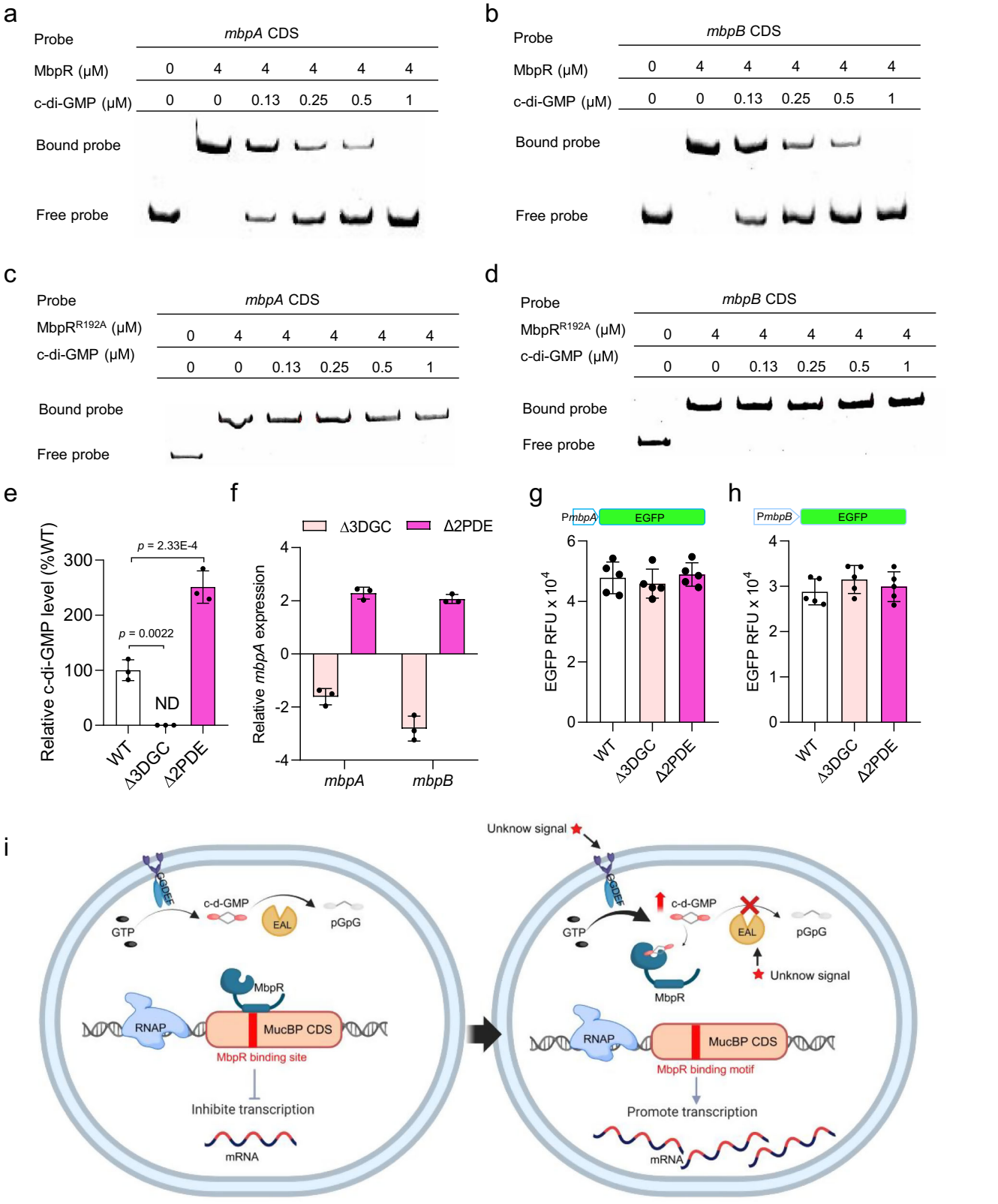

primers listed in Supplementary Data 7. The abovementioned gRNA and homologous arms were cloned into pHSP02 digested with ApaI and XbaI by using In-Fusion cloning. Then, *L. plantarum* WCFS1 containing pLH01 plasmid was cultured to an OD_{600} of 0.3. The inducing peptide (amino acid sequence: MAGNSSNFIHKIKQIFTHR, synthesized by GenScript Biotech Corp., China) was added (final concentration of 100 ng/mL) to induce the expression of RecE/T until OD_{600} reached 0.6. Then, the cells were generated into electrocompetent cells and transformed with 1.0 μg pHSP plasmids (listed in Supplementary Data 6) followed by 2-3 h recovery at 30 °C. The recovery mixture was plated on the MRS agar plate supplemented with 10 μg/mL erythromycin and 10 μg/mL chloramphenicol and incubated at 30°C for colony formation. The mutants were screened by PCR using primers listed in Supplementary Data 7. The mutant was sub-cultured in MRS

Fig. 6 | c-di-GMP reversed the inhibitory effects of MbpR. a–**d** EMSA detection of MbpR (**a**, **b**) and MbpR^{R192A} (**c**, **d**) binding to the *mbpB* or *mbpA* coding DNA sequence (CDS) probe in the presence of different amounts of c-di-GMP. The probe was incubated with protein at room temperature for 30 min. The experiments were performed three times with similar results. **e** Intracellular c-di-GMP level of the wild type, Δ3DGC, and Δ2PDE mutants. **f** Relative *mbpA* and *mbpB* transcription level in Δ3DGC and Δ2PDE strains analyzed by RT-qPCR. **g**, **h** Fluorescence intensity of EGFP, which was expressed from the reporting plasmid under the control of *mbpA* (**g**) and *mbpB* (**h**) promoter, in the wild-type, Δ3DGC, and Δ2PDE strains. The Δ3DGC strain was constructed by deleting *dgcD, dgcC*, and *dgcB*. The Δ2PDE strain mutant was generated by deleting *pdeD* and *pdeA*. **i** A pathway for c-di-GMP mediating *L. plantarum* colonization (Created in BioRender. Zhang, J. (2025) https://BioRender.com/g28k816). At low c-di-GMP level, MbpR binds to the mucin-binding protein (MucBP) CDS and inhibits its transcription. After sensing unknown signals, the activated diguanylate cyclases or inhibited c-di-GMP phosphodiesterases maintain the intracellular c-di-GMP level at a high level. The elevated c-di-GMP level results in MbpR releasing from the CDS of MucBP and promotes MucBP expression, promoting the colonization of *L. plantarum*. RNAP: RNA polymerase. Data in (**e**–**h**) are presented as mean values ± standard deviations (SD). Error bars indicate the SD. Dots represent individual data. Statistical significance in (**e**, **g**, **h**) was analyzed using one-way Analysis of Variance (ANOVA) with Tukey's multiple-comparison test. In (**e**, **f**): $n = 3$ biological repeats, In (**g**, **h**): $n = 5$ biological repeats. Source data are provided as a Source Data file.

without antibiotics for two generations to cure the editing plasmids. Then, a fraction of the culture was streaked onto an MRS agar plate and incubated at 37 °C for 48 h. PCR was performed to ensure the successful curing of editing plasmids. For complementation analysis, the coding region of target gene with its native promoter was amplified by PCR using the primers listed in Supplementary Data 7 and cloned into the pLH01 digested with EcoRI. The generated plasmid was electroporated into the mutant as described above.

Chromatin immunoprecipitation sequencing (ChIP-Seq)

To construct the vectors for ChIP-Seq, the pP23-FLAG plasmid was generated by inserting a DNA fragment, which is synthesized by GENEWIZ Inc., containing the P23 promoter, a multiple cloning site, and a 3 × FLAG tag was cloned into the EcoRI site of pLH01 plasmid by In-Fusion cloning. The *mbpR* and *mbpR*^{R192A} were amplified from *L. plantarum* WCFS1 genomic DNA. The purified PCR products were cloned into the pP23-FLAG vector digested with EcoRI and NotI to generate pP23-*mbpR*-FLAG and pP23-*mbpR*^{R192A}-FLAG. The constructs were transformed into the Δ*mbpR* mutant by electroporation. ChIP assays were performed by Wuhan IGENEBOOK Biotechnology Co., Ltd[50]. Briefly, Δ*mbpR* containing pP23-*mbpR*-FLAG or pP23-*mbpR*^{R192A}-FLAG was grown in MRS to the logarithmic phase. Formaldehyde was added to the medium at a final concentration of 1% (vol/vol), and incubation for 30 min. Glycine (at a final concentration of 125 mM) was then added to stop the cross-linking. The samples were left at room temperature for 10 min and washed twice with phosphate-buffered saline buffer (pH 7.4). The pellets were resuspended and incubated at 37 °C for 25 min in 0.5 mL of lysis buffer (100 mM Tris-Cl, pH 8.0, 300 mM NaCl) which contains 15 mg/mL of lysozyme and 1 × protease inhibitor (Thermo Fisher Scientific, USA). Subsequently, 0.5 mL immunoprecipitation (IP) buffer (50 mM Tris-Cl, pH 8.0, 250 mM NaCl, 1% Triton X-100, 1 × protease inhibitor) was added. The samples were chilled on ice and sonicated to shear chromosomal DNA. The sheared chromatin was immunoprecipitated by 10 µg of Anti-DDDDK tag (Binds to FLAG® tag sequence) antibody [EPR20018-251] (Abcam, ab205606) at 4 °C for 12 h. Then, 30 µL of protein beads were added for further incubation for 3 h. The beads were next washed once with 20 mM Tris/HCL (pH 8.1), 50 mM NaCl, 2 mM EDTA, 1% Triton X-100, 0.1% SDS; twice with 10 mM Tris/HCL (pH 8.1), 250 mM LiCl, 1 mM EDTA, 1% NP-40, 1% deoxycholic acid; and twice with 1 × TE buffer (10 mM Tris-Cl at pH 7.5. 1 mM EDTA). The bound material was then eluted from the beads in 300 µL of elution buffer (100 mM $NaHCO_3$, 1% SDS), treated with RNase A (final concentration 8 µg/mL) for 6 h at 65 °C and then treated with proteinase K (final concentration 345 µg/mL) overnight at 45 °C. Immunoprecipitated DNA was used to construct sequencing libraries following the protocol provided by the NEXTFLEX ChIP-Seq Library Prep Kit for Illumina Sequencing (NOVA-5143-02, Bioo Scientific) and sequenced on an Illumina NovaSeq 6000 with the PE 150 method. Trimmomatic (version 0.38) was used to filter out low-quality reads[51]. The clean reads were mapped to the *L. plantarum* WCFS1 genome by Bwa (version 0.7.15)[52]. SAMtools (version 1.3.1) was used to remove potential PCR duplicates[53]. MACS2 software (version 2.1.1.20160309) was used to call peaks by default parameters (bandwidth, 300 bp; model fold, 5, 50; q value, 0.05). If the summit of a peak was located closest to the transcription start site (TSS) of one gene, the peak was assigned to that gene[54]. MEME (version 3) was used to predict motif occurrence within peaks with default settings for a maximum motif length of 12 base pairs[55].

Overexpression of RocR and WspR

To overexpress *rocR* and *wspR* in *L. plantarum* WCFS1, the open reading frames (ORF) of the two genes were amplified from *P. aeruginosa* PAO1 genomic DNA and cloned into the EcoRI and the NotI site of pP23-FLAG vector by In-Fusion cloning. The generated pP23-*rocR*-FLAG and pP23-*wspR*-FLAG were transformed into the wild-type strain of *L. plantarum* WCFS1 by electroporation.

Electrophoretic mobility shift assay (EMSA)

Briefly, the DNA fragments or promoters were amplified by using primers listed in Supplementary Data 7 and purified by EZNA Cycle-Pure Kit (Omega Bio-tek, USA). PCR products were labeled by biotin using Biotin 3′ End DNA Labeling Kit (Thermo Fisher Scientific, USA). The binding reactions were performed in EMSA buffer (100 mM Tris pH 8.0, 10% glycerol, 300 mM NaCl, 50 mM $MgCl_2$) in the presence of indicated concentrations of protein and 50 ng of DNA probes. When required, the indicated amount of c-di-GMP was added. The mixture was incubated for 30 min at 37 °C and then sampled to a 5% polyacrylamide gel. After electrophoresis in 0.5 × TBE buffer at 4 °C, the DNA probe was transferred to the nylon membrane. The protein-DNA complex was crosslinked by UV. The probes were detected using the biotin luminescence detection kit (Thermo Fisher Scientific, USA) and imaged by ChemiDoc Imaging Systems (Bio-Rad, USA).

Extraction and quantification of intracellular c-di-GMP

Bacteria cells were grown to mid-log phase ($OD_{600} = 1.0$) and harvested by centrifugation. The pellet was washed with cooled water followed by treatment with 0.6 M of perchloric acid (Sigma)[56]. The pH of the soluble fraction was adjusted with $KHCO_3$. After centrifugation at 20,000 g for 5 min, the resulting supernatant was filtered, and c-di-GMP levels were measured using LC-MS/MS. The samples were separated on a UPLC Waters HSS T3 column (100 mm × 2.1 mm, 1.8 µm) using a binary pump system with solvent A (water containing 0.1% (v/v) formic acid) and eluent B (methanol containing 0.1% (v/v) formic acid). The gradient started at 12% eluent B and was held for 10 min at a flow rate of 0.3 mL/min. The analyte detection was carried out on a hybrid LCMS-IT-TOF liquid chromatograph mass spectrometer from Shimadzu (Kyoto, Japan) or an AB SCIEX Triple Quad™ 6500 system in positive ionization mode. The mass spectrometry parameters of LCMS-IT-TOF were set as follows: spray voltage, 4.50 kV; detector voltage, 1.65 kV; ion accumulation time, 20 ms; N_2 flow, 1.5 L/min; drying gas, 100.0 kPa; heat block temperature, 200 °C; CDL temperature, 200 °C; TOF pressure, 1.8×10^{-4} Pa; IT pressure, 1.8×10^{-2} Pa; RP vacuum, 70.0 Pa; mass range was set from 350 to 1000 Da. The mass spectrometry parameters of Triple Quad 6500+ were set as follows: ion

source gas 1, 50 psi; ion source gas 2, 50 psi; curtain gas, 25 psi; collision gas, high; positive ion spray voltage, 5500 V; source temperature, 500 °C. The following three mass transitions were detected in multiple reaction monitoring (MRM) model: 691 → 152 (qualifier), 691 → 540, and 691 → 248.

Protein purification

Briefly, target genes were amplified by using primers listed in Supplementary Data 7 and *L. plantarum* WCFS genomic DNA as the template. The PCR products were purified and cloned into the pET-28a vector. The fusion gene constructs were then transformed into *E. coli* strain BL21(DE3) for expression. After incubating the cultures at 37 °C to an OD_{600} of 0.5, isopropyl-*β*-d-thiogalactoside (IPTG) at a final concentration of 1 mM was added. The cells were grown overnight at 16 °C and collected by centrifugation. The pellet was resuspended in Lysis buffer (100 mM Tris-HCl, pH 8.0, 300 mM NaCl) and was lysed by sonication. The lysate was then centrifuged at 4 °C, and the 6 × His fusion proteins were purified from the supernatant by using Ni-NTA resin (Thermo Fisher Scientific, USA). Finally, the His-tag was removed using thrombin enzyme.

Affinity pull-down assay

Screening of c-di-GMP effector protein in *L. plantarum* WCFS1 was performed using affinity pull-down method[57]. Briefly, *L. plantarum* WCFS1 was inoculated in 100 mL of MRS supplemented with 0.2 M sucrose and 3 % glycine. The cells were grown at 37 °C until OD_{600} = 0.6, and then were harvested by centrifugation. The pellet was re-suspended with 1 mL binding buffer [100 mM Tris-HCl buffer (pH 7.5), 300 mM NaCl, 10 mM $MgCl_2$, 0.5 mM DTT, 0.5% (vol/vol) Triton X-100, 1 × protease inhibitor, 1% (vol/vol) n-dodecyl-β-D-Maltopyranoside], which was subjected to disruption by ultrasonication. The supernatant was collected after centrifugation. Then, biotinylated c-di-GMP (B098, BioLog, USA) at a final concentration of 10 μM was added to 100 μg of soluble protein. The mixture was incubated at 4 °C overnight. Streptavidin dynabeads (Thermo Fisher Scientific, USA) were added to capture the biotin-c-di-GMP for 30 min and were repeatedly washed thrice with binding buffer. After each washing, the supernatant was removed. Then, the streptavidin dynabeads were resuspended in protein loading buffer and boiled for 5 min. The supernatant was used for SDS-PAGE analysis. The experiments were performed three times and all PAGE gels were collected and cut into 1–2 mm gel particles. After washing with ethanol-acetic acid-water (4:1:5, v/v), the gel particles were subjected to dehydration by 500 μL of acetonitrile twice. 10 mM DTT (1 M DTT: 25 mM NH_4HCO_3 = 1:100) was added and incubation at 56 °C for 1 h. The liquid was removed and 55 mM iodoacetamide (IAM) (0.55 M IAM:25 mM NH_4HCO_3 = 1:10) was added. After incubation for 45 min at room temperature in dark environment, the particles were dehydrated by acetonitrile again and digested by 0.01 μg/μL with 25 mM NH_4HCO_3 with Trypsin overnight at 37 °C. The resulting peptides were separated by Easy-nLC 1200 (Thermo Fisher Scientific, USA) with self-packed C18 column (75 μm internal diameter, 1.9 μm column size, 25 cm column length) at a flow rate of 200 nL/min by the following effective gradient: 0–3 min, 5% mobile phase B (80% acetonitrile, 0.1% formic acid); 3–45 min, mobile phase B linearly increased from 8% to 44%; 45–50 min, mobile phase B rose from 44% to 60%; At 50-53 min, mobile phase B rose from 60% to 100%; 53–60 min, 80% mobile phase B. The nanoliter liquid phase separation end was directly connected to the mass spectrometer. The separated peptides were ionized by a nanoESI source and then passed to a tandem mass spectrometer Oritrap Exploris 480 (Thermo Fisher Scientific, USA) for data dependent acquisition mode detection. The main parameters were set: ion source voltage was set to 2.1 kV, MS1 mass spectrometer scanning range was 350 ~ 1600 m/z; resolution was set to 60,000; MS2 starting m/z was fixed at 100. The ion screening conditions for MS2 fragmentation: charge 2^+ to 7^+, and the first second parent ions with the peak intensity exceeding 50,000. The ion fragmentation mode was HCD. The dynamic exclusion time was set to 30 seconds. The AGC was set to: MS1 1E6, MS2 1E5. Results from search engine were pre-processed and re-scored using Percolator (V2.04) to improve the matching accuracy. The output was then filtered by FDR 1% at spectral level (PSM-level FDR ≤ 0.01) to obtain a significant identified spectrum and peptide list. The Mascot 2.3.02 search engine was used to identify proteins with more than 3 unique peptides based on UniProt protein database. LC-MS analysis was performed once.

Measurement of fluorescence

To generate the EGFP reporting plasmids, the *egfp* and the promoter of *mbpA* or *mbpB* were amplified from pAb-*egfp*[23] and *L. plantarum* WCFS1 genomic DNA, respectively. The fragments were cloned into the EcoRI site of pLH01. To detect the EGFP expression under the control of *mbpA* or *mbpB* promoter in the *mbpR* complementary mutant, a fragment containing *mbpA* or *mbpB* promoter, *egfp*, and *mbpR* with its native promoter was amplified by overlap extension PCR and cloned into the EcoRI site of pLH01. To determine the expression of EGFP and mCherry under the control of P23 promoter, a fragment containing the MbpR-binding sequence of *mbpA* between *egfp* and *mCherry* was amplified by using overlap extension PCR and cloned into the pP23-FLAG vector digested with EcoRI and NotI. The ORF of mCherry was amplified from pT7-6 × His-MCS-mCherry vector (Miaolingbio, China). To determine the expression of EGFP and mCherry fusing protein in the *mbpR* complementary strain, the DNA fragment of *mbpR* with its native promoter and the fragment containing *egfp*, MbpR-binding sequence of *mbpA*, and *mCherry* were cloned into the pP23-FLAG vector digested with EcoRI and NotI. The generated reporting plasmids were transformed into *L. plantarum* by electroporation. Bacterial colonies containing reporter plasmids were picked and grown to OD_{600} = 1.0 in MRS supplemented with 10 μg/mL of chloramphenicol at 37 °C. Cells were collected by centrifugation and washed with 3 × PBS. The signal of fluorescent protein was measured by Multimode Microplate Reader Synergy H1 (BioTek, USA) and normalized to the OD_{600} at the time of sampling.

Western blot

The DNA fragments containing FLAG-tagged *mbpR* and *rpoD* with their respective promoters were amplified and cloned into the pLH01 plasmid digested with EcoRI. To determine the expression of MbpR from the pP23-*mbpR*-FLAG plasmid used for ChIP-Seq, another plasmid (pP23-*mbpR*-FLAG-*rpoD*) was constructed by the addition of a FLAG-tagged *rpoD* fragment in the NheI cutting site of pP23-*mbpR*-FLAG vector. The reconstructive plasmids were transformed into Δ*mbpR* by electroporation and the levels of FLAG-tagged proteins were detected by using western blot. Briefly, cells (strains used for WB were listed in Supplementary Data 6) were grown to logarithmic growth phase (OD_{600} = 1.0) and were collected by centrifugation. After rinsing three times with PBS, the pellets were resuspended in 100 μL of Laemmli buffer, and boiled for 5 min. 20 μL of samples were run on 10% SDS-PAGE gels and transferred onto polyvinylidene fluoride membranes. The membranes were blocked in Tris-buffered saline containing 0.5% Tween 20 (TBST) and 5% non-fat milk, followed by overnight incubation with the Anti-DDDDK tag (Binds to FLAG® tag sequence) antibody [EPR20018-251] (Abcam, ab205606, diluted 1:1000) in blocking buffer at 4 °C. After three washes with TBST, the membranes were incubated with HRP-labeled Goat Anti-Rabbit IgG (Beyotime, A0208, diluted 1:1000) in TBST for 2 h. The bands were visualized by using SignalFire ECL Reagent (Cell Signaling Technology, USA).

In vitro transcription assay

The *mbpA* CDS region with T7 promoter was amplified using primers listed in Supplementary Data 7. The products were purified and 1 μg of

the product was used as transcription template for in vitro transcription assay. In vitro transcription assay was performed by using the T7 Quick High Yield RNA Transcription Kit (Beyotime, China) as described by the manufacturer in a final volume of 20 µL. The reaction was initiated by the addition of templates and incubated for indicated times at 37 °C. Synthesized RNAs were purified and quantified using nanodrop (Thermo Fisher Scientific, USA).

Bacterial two-hybrid assay (BTHA)

BTHA is based on the reconstitution of adenylate cyclase activity in *E. coli* BTH101[58]. The *mbpR* was amplified from *L. plantarum* WCFS1 genomic DNA and cloned into the pUT18 digested with HindIII and EcoRI. The *mbpR* and *rpoD* were amplified from *L. plantarum* WCFS1 genomic DNA and cloned into the pKNT25 digested with HindIII and EcoRI. To test protein-protein interactions, the pair of plasmids were co-electroporated into BTH101. The cells were grown on LB agar plates containing 100 µg/mL ampicillin, 50 µg/mL kanamycin, 0.5 mM IPTG, and 40 µg/L 5-bromo-4-chloro-3indolyl-β-D-galactopyranoside (X-gal) for 48 h at 30 °C. The interactions were then analyzed by the formation of blue clones.

RNA-Seq analysis

High-throughput RNA-Seq was performed by using double-stranded cDNA[59]. Double biological replicates were sequenced for each strain. The trimmed sequence reads were aligned to the *L. plantarum* WCFS1 genome sequence using Bowtie2-2.2.3[60], and the normalized read counts were compared by HTSeq v0.6.1[61]. Then, the FPKM of each gene was calculated based on the 26 lengths of this gene, and the read count was mapped to the gene[61]. Differentially expressed genes were identified as those with a high or low expression level (absolute value of $\log_2$ Fold Change was ≥1.5, $p < 0.05$) across all replicates with a false discovery rate (FDR) of <0.01.

Site-directed Mutagenesis

The sequences encoding protein mutants were generated by an overlapping PCR mutagenesis approach. Then, the purified PCR product was cloned into vector pET28a using In-Fusion cloning. After verification by DNA sequencing, all mutations plasmids were transformed into *E. coli* BL21 (DE3) strain, and the mutant proteins were expressed and purified using the same protocol described above.

Molecular docking analysis

To construct the 3D model, the protein sequence of MbpR (accession no: WP_011100868.1) was downloaded from the GenBank database in FASTA format and was submitted to the AlphaFold server (https://golgi.sandbox.google.com/). The output of the predicted model generated as a PDB file was downloaded for further analysis. 3D structure of c-di-GMP was extracted from the complex of syn_CdgR-(c-di-GMP) (PDB: 8HJA)[62] by pymol. Molecular docking was performed by using AUTODOCK tools 1.5.6 (http://www.scripps.edu/mb/olson/doc/Autodock). Before docking, polar-H atoms were added to the target protein and c-di-GMP, and Gasteiger charge calculations were performed. The molecule files were then saved in PDBQT format. Ligand-centered maps were generated by the AutoGrid program with a spacing of 0.368 Å and grid dimensions of 126 × 126 × 126 Å3. To screen the potential binding sites, the grid box was prepared to wrap the entire WYL domain. The receptor grid was centered at center_x = 8.641, center_y = 1.573, center_z = -13.284, size_x = 20.83, size_y = 26.25, size_z = 26.25. The exhaustiveness was set at 50. The conformation with the lowest binding energy was chosen and the potential ligand-protein interaction was calculated by the protein-ligand interaction profiler (https://plip-tool.biotec.tu-dresden.de/plip-web/plip/index). Finally, the surface representation of the structural model of MbpR in complex with c-di-GMP and the potential amino acids of MbpR involved in c-di-GMP binding was visualized by Pymol.

RT-qPCR

Strains including WT(pLH01), Δ*mbpR*(pLH01), Δ*mbpR*(*mbpR*) were cultured to OD_{600} = 1.0 and then harvested. RNA was isolated using a TRIZOL Reagent (Thermo Fisher Scientific, USA). cDNA synthesis and RT-qPCR analysis were performed with ChamQ™ Universal SYBR qPCR Master Mix (Vazyme, Nanjing, China) according to the manufacturer's instructions in a qTOWER 3 G (Analytic Jena, Jena, Germany). The expression levels of target genes were normalized to the level of the 16S RNA transcript for each experiment. The relative expression levels of the target genes were calculated using the comparative CT ($2^{-\Delta\Delta CT}$) method[63].

Isothermal titration calorimetry (ITC) assay

The experiments were performed on MicroCal PEAQ-ITC microcalorimeter (Malvern Panalytical GmbH, Germany). Both the c-di-GMP (Sigma-Aldrich) and protein were dissolved in Tris buffer (100 mM Tris-HCl, 300 mM NaCl, pH 8.0). Titrations began with one injection of 0.4 µL of c-di-GMP (500 µM) solution into MbpR solution (50 µM) in the calorimeter cell at 25 °C. The volume of c-di-GMP injection was changed to 3 µL in the subsequent twelve injections. The data were calibrated with a buffer control. The instrument software (MicroCal PEAQ-ITC Analysis Software) was used for baseline adjustment, peak integration, and normalization of the reaction heats with respect to the molar amount of injected ligand as well as for data analysis and binding parameter evaluation.

Enzyme activity assays

DGC and PDE activity assays were performed with 10 µM purified protein (final concentration) in a final volume of 40 µL of reaction buffer [100 mM Tris-HCl (pH 8.0), 300 mM NaCl, 10 mM $MgCl_2$] at 37 °C. The reactions were induced by adding GTP or c-di-GMP at a final concentration of 0.1 mM followed by heating for 5 min at 100 °C. The products were detected by a high-performance liquid chromatography (HPLC) instrument equipped with a UV/Vis detector set to 253 nm. Separation was carried out using a reverse-phase C18 Waters column (4.6 × 250 mm; 5 µm) and a flow rate of 1 mL/min. Solvents containing methanol and 10 mM ammonium acetate at a ratio of 1/9 (v/v) were used.

Microscale thermophoresis (MST) assay

The protein binding affinities to c-di-GMP and other ligands were assessed by a Nano Temper 16 Monolith NT.115 instrument (Nano-Temper technologies, Germany). In brief, purified proteins were labeled with the L001 Monolith NT.115 Protein Labeling Kit (Nano Temper). A mixture of labeled protein and varying concentrations of unlabeled c-di-GMP was prepared and loaded into standard treated silicon 19 capillaries (K002 Monolith NT.115. The fluorescence readings were acquired by a Nano Temper 16 Monolith NT.115 instrument, with measurements conducted at 20% LED power and 40% MST power.

Acid and bile salt tolerance assay

The cells of cultures growing in MRS were harvested by centrifugation at 4500 g for 10 min and then washed twice in PBS. Cell pellets were resuspended with MRS broth with different pH values or containing various concentrations of taurocholic acid sodium salt. The mixture was incubated at 37 °C for 2 h. The viable count was carried out on MRS agar, and the survival rate (%) was calculated.

Cell adhesion experiments

HT-29 cell (CBP60011) obtained from Nanjing Cobioer Biosciences Co. Ltd. was used to test the adhesive ability of *L. plantarum*. Cells (5×10^5 cells/mL) were seeded in a 96-well culture plate and incubated at 37 °C under 5% CO_2 until the cells reached full confluence. *L. plantarum* was cultured until reaching mid-log phase. The bacterial cells were collected and washed twice with PBS, and then suspended in DMEM to

obtain a final concentration of 10^8 CFU/mL. After washing the HT-29 cells twice with PBS, the bacterial suspension was added to each well and incubated for 2 h. Cells containing attached bacteria were rinsed thrice with PBS and lysed by incubating with 1% (v/v) Triton X-100 at 4 °C for a duration of 20 min. The quantity of adhered *L. plantarum* was determined by plating serial dilutions of the lysed cells on MRS plates, followed by colony counting after incubation at 37 °C for 24 h.

Animal experiments

This study was approved by the Animal Ethics Committee of Hainan University (approval number: HNUAUCC-2024-00011), and all animal operations were carried out in accordance with the "Guidelines for The Care and Use of Experimental Animals" of Hainan University. As substantial researches have shown that male and female mice exhibit notable differences in metabolism, hormone levels, and immune responses[64–66], we thus only used male mice for experiments. Six-week-old male C57 BL/6 mice were purchased from Guangdong Vital River Laboratory Animal Technology. Randomly allocated mice of each group ($n = 5$ per group) were maintained at an ambient temperature of 25 ± 2 °C, relative humidity of 55% ± 5%, and a 12-hour light-dark cycle. The mice were allowed to drink and eat freely. The diet used is provided by Jiangsu Xietong Pharmaceutical Bio-Engineering Co., Ltd., catalog number XTI01WC-009. The main composition of the diet includes moisture ≤100 g/kg, crude protein ≥180 g/kg, crude fat ≥40 g/kg, crude fiber ≤50 g/kg, crude ash ≤80 g/kg, total phosphorus ranging from 6 to 12 g/kg, and calcium content between 10 and 18 g/kg. Additionally, the diet contains significant levels of vitamins such as vitamin A (13692 IU/kg), vitamin D (1339 IU/kg), and vitamin E (115.4 mg/kg). The total energy content is 3790 Kcal/kg, with a physiological energy of 3408 Kcal/kg. The protein, fat, and carbohydrate supply ratios are 21.5%, 11.1%, and 67.4%, respectively. Mice were fasted for 12 h before the experiment and then were gavaged with 5×10^8 CFU of bacterial solution or an equal volume of MRS. The mice were euthanized by decapitation after 6 h of gavage, and the colon was collected at a length of 2 cm. After lavage trice with sterile PBS, the colon was stirred with a homogenizer. The samples were diluted and plated on MRS agar containing tetracycline (10 μg/mL), streptomycin (10 μg/mL), kanamycin (50 μg/mL), chloramphenicol (10 μg/mL) and vancomycin (30 μg/mL). Plates were placed in an incubator at 37 °C for 48 h to form single colonies.

Statistics & reproducibility

The data are presented as the means ± standard deviations (SDs) from at least three independent experiments and analyzed using Prism 8 software (GraphPad). The error bars indicate the SD. Dots represent individual data. Biological replicates and numbers of independent experiments were stated in the legends. Statistical significance was performed using one-way ANOVA with Tukey's multiple-comparison test.

Data availability

All the data that support the findings of this study are available within the paper and its Supplementary Data. The mass spectrometry proteomics data have been deposited to the ProteomeXchange Consortium via the PRIDE partner repository with the dataset identifier PXD053948. The RNA-seq and ChIP-seq data generated in this study have been deposited in the National Center for Biotechnology Information Sequence Read Archive (SRA) database under accession code PRJNA1197435 and PRJNA1129814, respectively. The protein 3D structure data used in this study are available in the AlphaFold database under accession codes F9USQ8. The structure of c-di-GMP used in this study is available in the PDB database under accession code 8HJA. Source data are provided with this paper.

References

1. Zhang, Q. et al. *Lactobacillus plantarum*-derived indole-3-lactic acid ameliorates colorectal tumorigenesis via epigenetic regulation of $CD8^+$ T cell immunity. *Cell Metab.* **35**, 943–960.e949 (2023).
2. Yang, N. et al. *Lactiplantibacillus plantarum* P9 for chronic diarrhea in young adults: a large double-blind, randomized, placebo-controlled trial. *Nat. Commun.* **15**, 6823 (2024).
3. Wang, Y. et al. *Lactiplantibacillus plantarum* HNU082 inhibited the growth of *Fusobacterium nucleatum* and alleviated the inflammatory response introduced by *F. nucleatum* invasion. *Food Funct.* **12**, 10728–10740 (2021).
4. Wu, Y. et al. *Lactobacillus plantarum* HNU082 alleviates dextran sulfate sodium-induced ulcerative colitis in mice through regulating gut microbiome. *Food Funct.* **13**, 10171–10185 (2022).
5. Paone, P. & Cani, P. D. Mucus barrier, mucins and gut microbiota: the expected slimy partners? *Gut* **69**, 2232–2243 (2020).
6. Jin, H. et al. A high-quality genome compendium of the human gut microbiome of Inner Mongolians. *Nat. Microbiol* **8**, 150–161 (2023).
7. Alp, D. & Kuleaşan, H. Adhesion mechanisms of lactic acid bacteria: conventional and novel approaches for testing. *World J. Microbiol. Biotechnol.* **35**, 156 (2019).
8. Han, S. et al. Probiotic gastrointestinal transit and colonization after oral administration: A long journey. *Front. Cell. Infect. Microbiol.* **11**, 609722 (2021).
9. Singhal, N., Singh, N. S., Mohanty, S., Kumar, M. & Virdi, J. S. Rhizospheric *Lactobacillus plantarum* (*Lactiplantibacillus plantarum*) strains exhibit bile salt hydrolysis, hypocholestrolemic and probiotic capabilities in vitro. *Sci. Rep.* **11**, 15288 (2021).
10. Tennant, S. M. et al. Influence of gastric acid on susceptibility to infection with ingested bacterial pathogens. *Infect. Immun.* **76**, 639–645 (2008).
11. Zmora, N. et al. Personalized gut mucosal colonization resistance to empiric probiotics is associated with unique host and microbiome features. *Cell* **174**, 1388–1405.e1321 (2018).
12. Romling, U., Galperin, M. Y. & Gomelsky, M. Cyclic di-GMP: the first 25 years of a universal bacterial second messenger. *Microbiol. Mol. Biol. Rev.* **77**, 1–52 (2013).
13. Chou, S. H. & Galperin, M. Y. Diversity of cyclic di-GMP-binding proteins and mechanisms. *J. Bacteriol.* **198**, 32–46 (2016).
14. Obeng, N. et al. Bacterial c-di-GMP has a key role in establishing host-microbe symbiosis. *Nat. Microbiol.* **8**, 1809–1819 (2023).
15. Khan, F., Jeong, G. J., Tabassum, N. & Kim, Y. M. Functional diversity of c-di-GMP receptors in prokaryotic and eukaryotic systems. *Cell Commun. Signal* **21**, 259 (2023).
16. Laventie, B. J. et al. A surface-induced asymmetric program promotes tissue colonization by *Pseudomonas aeruginosa*. *Cell Host Microbe* **25**, 140–152 (2019).
17. Rick, T. et al. GGDEF domain as spatial on-switch for a phosphodiesterase by interaction with landmark protein HubP. *NPJ Biofilms Microbiomes* **8**, 35 (2022).
18. Newell, P. D., Monds, R. D. & O'Toole, G. A. LapD is a bis-(3′,5′)-cyclic dimeric GMP-binding protein that regulates surface attachment by *Pseudomonas fluorescens* Pf0-1. *Proc. Natl Acad. Sci. U.S.A.* **106**, 3461–3466 (2009).
19. Matsuyama, B. Y. et al. Mechanistic insights into c-di-GMP-dependent control of the biofilm regulator FleQ from *Pseudomonas aeruginosa*. *Proc. Natl Acad. Sci. Usa.* **113**, E209–E218 (2016).
20. Floyd, K. A. et al. c-di-GMP modulates type IV MSHA pilus retraction and surface attachment in *Vibrio cholerae*. *Nat. Commun.* **11**, 1549 (2020).
21. Kaczmarczyk, A. et al. Precise timing of transcription by c-di-GMP coordinates cell cycle and morphogenesis in *Caulobacter*. *Nat. Commun.* **11**, 816 (2020).

22. Shanahan, C. A., Gaffney, B. L., Jones, R. A. & Strobel, S. A. Differential analogue binding by two classes of c-di-GMP riboswitches. *J. Am. Chem. Soc.* **133**, 15578–15592 (2011).
23. Guo, Q. et al. Elongation factor P modulates *Acinetobacter baumannii* physiology and virulence as a cyclic dimeric guanosine monophosphate effector. *Proc. Natl Acad. Sci. Usa.* **119**, e2209838119 (2022).
24. Shyp, V. et al. Reciprocal growth control by competitive binding of nucleotide second messengers to a metabolic switch in *Caulobacter crescentus*. *Nat. Microbiol.* **6**, 59–72 (2021).
25. Keller, L. M. L., Flattich, K. & Weber-Ban, E. Novel WYL domain-containing transcriptional activator acts in response to genotoxic stress in rapidly growing mycobacteria. *Commun. Biol.* **6**, 1222 (2023).
26. Keller, L. M. & Weber-Ban, E. An emerging class of nucleic acid-sensing regulators in bacteria: WYL domain-containing proteins. *Curr. Opin. Microbiol.* **74**, 102296 (2023).
27. Andis, N. M., Sausen, C. W., Alladin, A. & Bochman, M. L. The WYL domain of the PIF1 helicase from the thermophilic bacterium *Thermotoga elfii* is an accessory single-stranded DNA binding module. *Biochemistry* **57**, 1108–1118 (2018).
28. Müller, A. U., Leibundgut, M., Ban, N. & Weber-Ban, E. Structure and functional implications of WYL domain-containing bacterial DNA damage response regulator PafBC. *Nat. Commun.* **10**, 4653 (2019).
29. Blankenchip, C. L. et al. Control of bacterial immune signaling by a WYL domain transcription factor. *Nucleic Acids Res* **50**, 5239–5250 (2022).
30. Picton, D. M. et al. A widespread family of WYL-domain transcriptional regulators co-localizes with diverse phage defence systems and islands. *Nucleic Acids Res.* **50**, 5191–5207 (2022).
31. Hengge, R. Principles of c-di-GMP signalling in bacteria. *Nat. Rev. Microbiol.* **7**, 263–273 (2009).
32. Sauvaitre, T. et al. Role of mucus-bacteria interactions in enterotoxigenic *Escherichia coli* (ETEC) H10407 virulence and interplay with human microbiome. *NPJ Biofilms Microbiomes* **8**, 86 (2022).
33. Drexler, D. J., Müller, M., Rojas-Cordova, C. A., Bandera, A. M. & Witte, G. Structural and biophysical analysis of the soluble DHH/DHHA1-type phosphodiesterase TM1595 from *Thermotoga maritima*. *Structure* **25**, 1887–1897.e1884 (2017).
34. Schumacher, M. A. et al. Structure of the WYL-domain containing transcription activator, DriD, in complex with ssDNA effector and DNA target site. *Nucleic Acids Res* **52**, 1435–1449 (2024).
35. Müller, A. U., Kummer, E., Schilling, C. M., Ban, N. & Weber-Ban, E. Transcriptional control of mycobacterial DNA damage response by sigma adaptation. *Sci. Adv.* **7**, eabl4064 (2021).
36. Römling U., Liang Z. X. & Dow J. M. Progress in understanding the molecular basis underlying functional diversification of cyclic dinucleotide turnover proteins. *J. Bacteriol.* **199**, e00790-16 (2017).
37. Makarova, K. S., Anantharaman, V., Grishin, N. V., Koonin, E. V. & Aravind, L. CARF and WYL domains: ligand-binding regulators of prokaryotic defense systems. *Front. Genet.* **5**, 102 (2014).
38. Hein, S., Scholz, I., Voß, B. & Hess, W. R. Adaptation and modification of three CRISPR loci in two closely related cyanobacteria. *RNA Biol.* **10**, 852–864 (2013).
39. Hua, C. et al. Bacterial transcription factors bind to coding regions and regulate internal cryptic promoters. *mBio* **13**, e0164322 (2022).
40. Jonkers, I. & Lis, J. T. Getting up to speed with transcription elongation by RNA polymerase II. *Nat. Rev. Mol. Cell Biol.* **16**, 167–177 (2015).
41. Bentley, D. L. Coupling mRNA processing with transcription in time and space. *Nat. Rev. Genet.* **15**, 163–175 (2014).
42. Liang, Z. X. The expanding roles of c-di-GMP in the biosynthesis of exopolysaccharides and secondary metabolites. *Nat. Prod. Rep.* **32**, 663–683 (2015).
43. Webster, S. S., Wong, G. C. L. & O'Toole, G. A. The power of touch: type 4 pili, the von willebrand a domain, and surface sensing by *Pseudomonas aeruginosa*. *J. Bacteriol.* **204**, e0008422 (2022).
44. Martínez-Gil, M., Ramos-González, M. I. & Espinosa-Urgel, M. Roles of cyclic di-GMP and the Gac system in transcriptional control of the genes coding for the *Pseudomonas putida* adhesins LapA and LapF. *J. Bacteriol.* **196**, 1484–1495 (2014).
45. Borlee, B. R. et al. Pseudomonas aeruginosa uses a cyclic-di-GMP-regulated adhesin to reinforce the biofilm extracellular matrix. *Mol. Microbiol* **75**, 827–842 (2010).
46. Koestler, B. J. & Waters, C. M. Bile acids and bicarbonate inversely regulate intracellular cyclic di-GMP in *Vibrio cholerae*. *Infect. Immun.* **82**, 3002–3014 (2014).
47. Heo, K. et al. Sugar-mediated regulation of a c-di-GMP phosphodiesterase in *Vibrio cholerae*. *Nat. Commun.* **10**, 5358 (2019).
48. Li, S. et al. Autoinducer-2 and bile salts induce c-di-GMP synthesis to repress the T3SS via a T3SS chaperone. *Nat. Commun.* **13**, 6684 (2022).
49. Huang, H., Song, X. & Yang, S. Development of a RecE/T-assisted CRISPR-Cas9 toolbox for *Lactobacillus*. *Biotechnol. J.* **14**, e1800690 (2019).
50. Landt, S. G. et al. ChIP-seq guidelines and practices of the ENCODE and modENCODE consortia. *Genome Res.* **22**, 1813–1831 (2012).
51. Bolger, A. M., Lohse, M. & Usadel, B. Trimmomatic: a flexible trimmer for Illumina sequence data. *Bioinformatics* **30**, 2114–2120 (2014).
52. Li, H. & Durbin, R. Fast and accurate short read alignment with Burrows-Wheeler transform. *Bioinformatics* **25**, 1754–1760 (2009).
53. Li, H. et al. The Sequence Alignment/Map format and SAMtools. *Bioinformatics* **25**, 2078–2079 (2009).
54. Salmon-Divon, M., Dvinge, H., Tammoja, K. & Bertone, P. PeakAnalyzer: genome-wide annotation of chromatin binding and modification loci. *BMC Bioinforma.* **11**, 415 (2010).
55. Machanick, P. & Bailey, T. L. MEME-ChIP: motif analysis of large DNA datasets. *Bioinformatics* **27**, 1696–1697 (2011).
56. Chua, S. L. et al. In vitro and in vivo generation and characterization of *Pseudomonas aeruginosa* biofilm-dispersed cells via c-di-GMP manipulation. *Nat. Protoc.* **10**, 1165–1180 (2015).
57. Skotnicka, D. et al. CdbA is a DNA-binding protein and c-di-GMP receptor important for nucleoid organization and segregation in *Myxococcus xanthus*. *Nat. Commun.* **11**, 1791 (2020).
58. Karimova, G., Pidoux, J., Ullmann, A. & Ladant, D. A bacterial two-hybrid system based on a reconstituted signal transduction pathway. *Proc. Natl Acad. Sci. USA* **95**, 5752–5756 (1998).
59. Yang, C. et al. *Burkholderia cenocepacia* integrates cis-2-dodecenoic acid and cyclic dimeric guanosine monophosphate signals to control virulence. *Proc. Natl Acad. Sci. Usa.* **114**, 13006–13011 (2017).
60. Langmead, B. & Salzberg, S. L. Fast gapped-read alignment with Bowtie 2. *Nat. Methods* **9**, 357–359 (2012).
61. Trapnell, C. et al. Transcript assembly and quantification by RNA-Seq reveals unannotated transcripts and isoform switching during cell differentiation. *Nat. Biotechnol.* **28**, 511–515 (2010).
62. Zeng, X. et al. A c-di-GMP binding effector controls cell size in a cyanobacterium. *Proc. Natl Acad. Sci. Usa.* **120**, e2221874120 (2023).
63. Livak, K. J. & Schmittgen, T. D. Analysis of relative gene expression data using real-time quantitative PCR and the 2(-Delta Delta C(T)) Method. *Methods* **25**, 402–408 (2001).
64. Wilkinson, N. M., Chen, H. C., Lechner, M. G. & Su, M. A. Sex differences in immunity. *Annu Rev. Immunol.* **40**, 75–94 (2022).
65. Sandovici, I., Fernandez-Twinn, D. S., Hufnagel, A., Constância, M. & Ozanne, S. E. Sex differences in the intergenerational inheritance of metabolic traits. *Nat. Metab.* **4**, 507–523 (2022).
66. Org, E. et al. Sex differences and hormonal effects on gut microbiota composition in mice. *Gut Microbes* **7**, 313–322 (2016).

Acknowledgements
This work was financially supported by the National Natural Science Foundation of China (No. 32222066) and the earmarked fund for Tropical High-efficiency Agricultural Industry Technology System of Hainan University (THAITS-4) awarded to J.Z.

Author contributions
Q.G., G.W., and J.Z. designed research; Q.G. and L.Z. performed research; J.Z. and G.W. contributed reagents/analytic tools; Q.G., L.Z., H.X, R.W., Y.F., and J.Z. analyzed data; Q.G., L.Z., and J.Z. wrote the paper.

Competing interests
The authors declare no competing interests.

Additional information
Supplementary information The online version contains supplementary material available at https://doi.org/10.1038/s41467-025-57581-4.

Correspondence and requests for materials should be addressed to Jiachao Zhang.

Peer review information *Nature Communications* thanks Kevin Gozzi, and the other, anonymous, reviewer for their contribution to the peer review of this work. A peer review file is available.